JOURNAL OF APPLIED PHYSICS

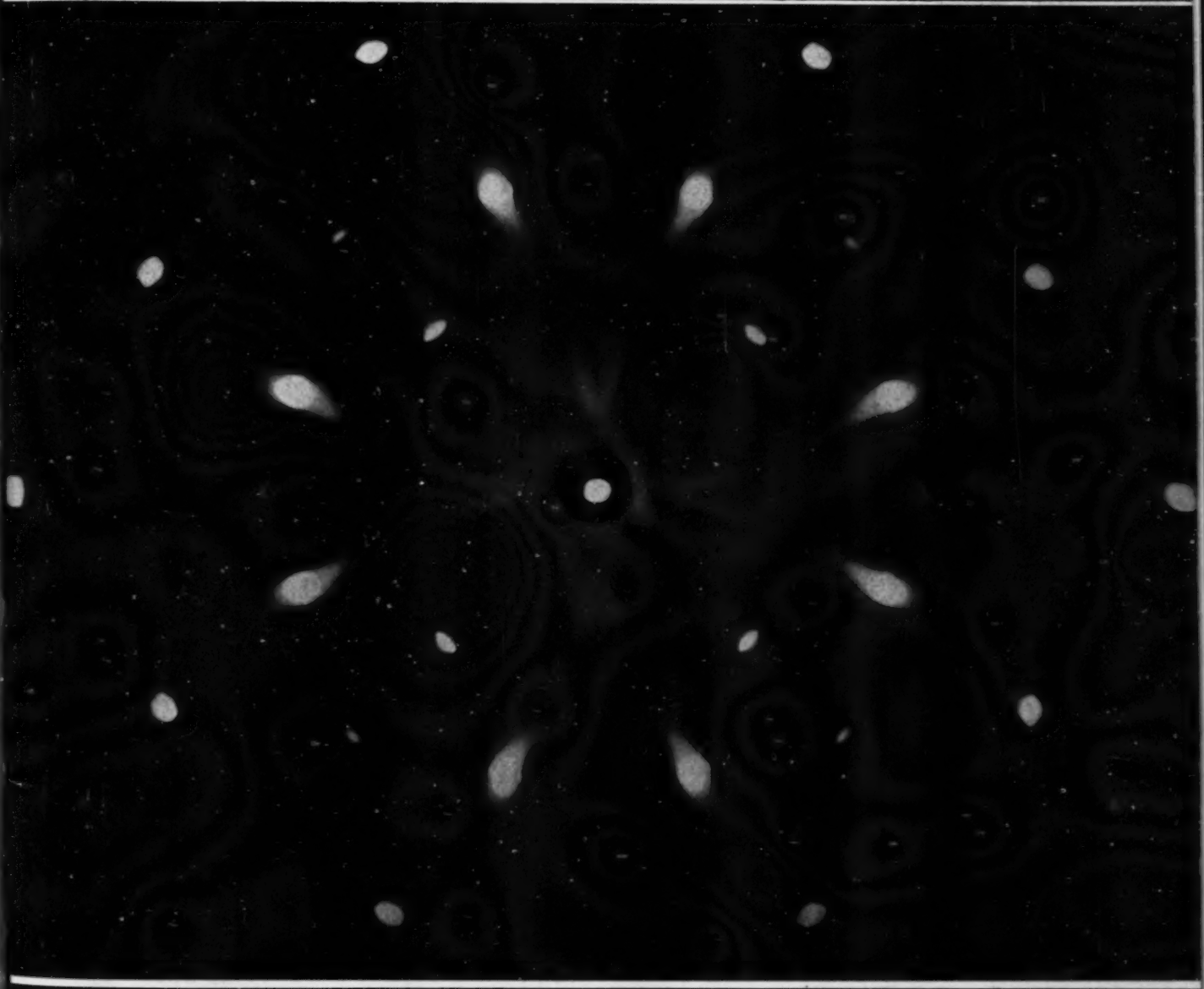

JOURNAL OF APPLIED

PHYSICS

NOVEMBER, 1940 Vol. 11, No. 11

In This Issue

Page

What Is a Physicist? 697

Flame Temperature
BERNARD LEWIS AND GUENTHER VON ELBE 698

Resumés of Recent Research 707

Contributed Original Research

Mechanical Model for the Motion of Electrons in a Magnetic Field
ALBERT ROSE 711

Notes on the Power Factor Testing of Long Lengths of Cables
ERIC A. WALKER 717

Similarity of the Stress Distributions in a Circular Disk and a Square Plate
H. ÔKUBO 720

Stress Analysis by Three-Dimensional Photoelastic Methods
DANIEL C. DRUCKER AND RAYMOND D. MINDLIN 724

Atomic Distribution in Aluminum-Silver Alloys During Aging
CHARLES S. BARRETT AND ALFRED H. GEISLER 733

Studies in Lubrication. IX. The Effect of the Pressure Variation of Viscosity on the Lubrication of Plane Sliders
M. MUSKAT AND H. H. EVINGER 739

In Every Issue

Here and There 708

Contributors to This Issue 710

Innovations in Instruments vi

Instrument Booklets viii

Index to Advertisers xii

BOARD OF EDITORS

ELMER HUTCHISSON,
Editor

Associate Editors

F. BITTER
W. E. FORSYTHE
L. A. JONES
B. E. WARREN
J. B. WHITEHEAD

Publication of the
American Institute of Physics

ADMINISTRATIVE STAFF

HENRY A. BARTON,
Director

MADELINE M. MITCHELL,
Publications Manager

JOHN T. TATE,
Adviser on Publications

GOVERNING BOARD

PAUL E. KLOPSTEG,
Chairman
GEORGE B. PEGRAM,
Secretary
KARL T. COMPTON
WHEELER P. DAVEY
FLOYD A. FIRESTONE
HARVEY FLETCHER
R. C. GIBBS
ARTHUR C. HARDY
GEORGE R. HARRISON
A. STUART HUNTER
H. R. LILLIE
FREDERIC PALMER, JR.
GEORGE B. PEGRAM
W. B. RAYTON
JOHN T. TATE
WALLACE WATERFALL

THE JOURNAL OF APPLIED PHYSICS, published monthly at Prince and Lemon Sts., Lancaster, Pa., is devoted to physics in its role as the science basic to other natural sciences and to the arts and industries. Previous to 1937 this publication was known as PHYSICS. It aims to be of service not only in physical laboratories, but also in the laboratories of industrial, chemical, geological, geophysical, meteorological, radio, and similar concerns. THE JOURNAL OF APPLIED PHYSICS publishes editorials, news of physicists and reviews, as well as technical papers of applied physics.

Manuscripts should be submitted to Elmer Hutchisson, Editor, University of Pittsburgh, Pittsburgh, Pennsylvania.

SUBSCRIPTION PRICE

	U. S., POSS. AND CANADA	FOREIGN
To members of scientific societies	$5.00	$5.70
To all others	7.00	7.70

Single copies are $.70 each.

Changes of address and proofs should be addressed to the Publications Manager.

Subscriptions and orders for back numbers should be addressed to Prince and Lemon Streets, Lancaster, Pa. or to the American Institute of Physics, 175 Fifth Avenue, New York, N. Y.

Advertising rates supplied on request. Orders, advertising copy and cuts should be sent to the American Institute of Physics.

Entered as second class matter at the Post Office at Lancaster, Pennsylvania, under the Act of March 3, 1897.
Accepted for mailing at the special rate of postage provided for in the Act of February 28, 1925, authorized May 2, 1932.

Copyright 1940, by the American Institute of Physics.

Journal of Applied Physics

Volume 11 November, 1940 Number 11

What is a Physicist?

RECENTLY, at a meeting of responsible Army, Navy and business officers to consider problems of national defense, the need for physicists to help in these problems was discussed. Several of those present spoke in no uncertain terms indicating that they had no need for men who dabbled only in atoms and who gave no thought to concrete problems whose immediate solution was required for the adequate defense of the country. This incident is mentioned since it illustrates very well the reputation which physicists have acquired in the minds of many of the leaders of our country.

The rather general belief that physicists are interested only in atoms probably has arisen because the progress in atomic and nuclear physics is so spectacular that newspapers print news in this field to the almost complete exclusion of news of any other work of the physicist. As a result, the painstaking care which the physicist has used in the establishment of precise standards of temperature, in the analysis of internal friction in vibrating rods, in the exact specification of color, in the development of optical instruments, in the design of electrical measuring instruments and in innumerable other projects of the greatest immediate importance has escaped the attention of those who are not directly concerned with the progress in physics.

This situation is unfortunate and is distinctly harmful to the development of physics as a profession. It often leads to the hiring of others to do the work that the physicist has been especially trained to do. One doesn't call in a dentist to treat pneumonia just because he has the title of doctor. Yet many an industrialist will call in any kind of technical man except the physicist to measure accurately the coefficient of expansion or to interpret an x-ray diffraction pattern or to carry out a spectroscopic analysis—jobs for which the physicist has more specific training than does the physician for the treatment of pneumonia.

What is the physicist to do about this? First of all, he must realize that no one else will do anything unless he makes the first move. It has been suggested that the first move is to formulate a comprehensive definition of the work of the physicist and then to make a concerted effort to bring this definition to the attention of the right people. To define the work of the physicist is not easy. Your editor will be pleased to receive suggestions for a concise but accurate definition of the physicist's work. Perhaps there are better ways to emphasize the broad nature of a physicist's interests. Further suggestions will be most welcome.

For December

Qualitative Spectrochemical Analysis in Agriculture and Geochemistry, **by STANLEY S. BALLARD.**

Also contributed research papers on:

Flow of Air Through Porous Media, Thermoplastic Behavior, Absorption Spectra, Theory of the Cyclotron, Noncubic Lattice Constants, Spark Gaps with Short Time Lag, and Isochronous Hairspring.

Flame Temperature*

By Bernard Lewis† and Guenther von Elbe‡

Central Experiment Station, Bureau of Mines, and the Coal Research Laboratory, Carnegie Institute of Technology, Pittsburgh, Pennsylvania

1. Introduction

IN this paper only flames produced incident to the use of fuels for heating and generation of power will be considered. If the fuel is in the gaseous state and is premixed with air or oxygen, after local ignition the burned and unburned gases are separated by a narrow reaction zone or flame front. If the fuel is discharged into the atmosphere combustion proceeds by interdiffusion of the gaseous or gasified fuel and the air. For organic fuels the latter flames are usually luminous because of formation of soot. This also applies to premixed flames with large excess of fuel.

Other luminous phenomena to which the term *flame* has been applied, such as the cool flames observed in the slow oxidation of gaseous hydrocarbons and in the interdiffusion of alkali metals and halogens do not warrant discussion here.

2. Theoretical and Experimental Flame Temperature

The quantity *temperature* defines a state of statistical equilibrium and can be assigned only to a system in which such an equilibrium exists. The *theoretical* flame temperature thus corresponds to the following postulated state of complete statistical equilibrium in the burned gas: Collisions between the molecules and radiation, although continually changing the state of every individual molecule, maintain on the average the randomness of direction of motion and the constancy of (a) the percentage of molecules possessing a given velocity; (b) the percentage of molecules possessing a given quantum state of rotation, of vibration, or of electronic excitation, and (c) the concentrations of dissociation products. The theoretical flame temperature can be calculated[1] for a given content of total energy of the gas from heat capacities and dissociation equilibria obtained by statistical-mechanical methods from band spectroscopic and other data. It is reasonable to assume that in all zones of an actual flame the equilibrium (a) in the translational degrees of freedom is established with close approximation because of the rapidity of the collision sequences; and since for perfect gases, which flame gases resemble, the temperature corresponding to this equilibrium is given by the gas law, an *experimental* flame temperature corresponding to the equilibrium in the translational degrees of freedom may always be obtained by determining the parameters of the gas law, pressure and molar volume. Whether the equilibrium (b) in the internal degrees of freedom and the chemical equilibrium (c) are also established with an approximation sufficient to eliminate measurable differences between theoretical and experimental flame temperatures remains to be investigated experimentally.

3. Comparison Between Theoretical and Experimental Flame Temperatures in Explosion Experiments

If an explosive gas mixture is ignited at the center of a spherical vessel, the resulting spherical flame does not come into contact with the cold walls of the vessel until combustion is complete, and the theoretical flame temperature can, in general, be calculated without difficult heat loss corrections. The maximum pressure established at the end of the explosion yields, on the other hand, the experimental flame temperature, the volume remaining constant. Experiments of this type have been carried out extensively for mixtures of hydrogen and oxygen with various

* Published by permission of the Director, Bureau of Mines, U. S. Department of the Interior, and the Director, Coal Research Laboratory, Carnegie Institute of Technology (not subject to copyright).

† Physical chemist, Explosives Division, Central Experiment Station, Bureau of Mines, Pittsburgh, Pa.

‡ Coal Research Laboratory, Carnegie Institute of Technology, Pittsburgh, Pa.

inert gases. It was found[1] that with the monatomic gases, argon and helium, as diluents the experimental and theoretical temperatures are identical within narrow limits of error, but that with diatomic gases, like excess oxygen or nitrogen, the experimental temperatures are appreciably higher than the theoretical. This indicates that the latter gases are slow to absorb energy in the internal degrees of freedom which they possess in distinction to the monatomic gases, and that equilibrium (b) is not established in the burned gas behind the flame front. The phenomenon has been referred to as excitation lag,[1] implying that the collisional excitation of the internal degrees of freedom, particularly those of vibration, is lagging behind the chemical reaction. Its occurrence suggests caution in the use of molecular infra-red radiation from flames for thermometric purposes, particularly if the emitting molecules are introduced into the mixture as diluent gas.

Such excitation lag is also noticeable in experiments with sound waves.[2] A large rotational excitation lag has recently been reported in the rapid compression of diatomic gases at room temperature[3] and the rapid discharge of steam through an orifice.[4]

4. *The Line-Reversal Method of Determining Flame Temperatures*

a. Theory

The line-reversal method of Féry[5] is based on the assumption that on introducing certain metal vapors into a flame statistical equilibrium is established between the electronic degrees of freedom of the metal atoms and the flame gases. The metal atoms thus emit and absorb their spectral lines as thermal radiators.

The quantity measured by the line-reversal method is brightness, B, defined by the equation

$$dE = B dA dt d\omega \cos\theta \qquad (1)$$

where dE is the energy radiated during the time dt from an element dA of the surface of a luminous body within the solid angle $d\omega$ at the angle θ to the normal. If the radiation is spectrally unresolved B is the *total brightness*. If only the energy dE_λ contained in the portion $d\lambda$ of the spectrum (λ being the wave-length) is considered, then

$$dE = B_\lambda d\lambda dA dt d\omega \cos\theta. \qquad (2)$$

B_λ is called the *spectral brightness*. Fundamental optics as well as thermodynamics show that the brightness B or B_λ of a body remains constant in the path of any individual light ray emitted by the body regardless of the interposition of lenses or mirrors, provided that the optical system is an ideal one, that is, there is no diffraction or absorption by lenses and mirrors or reflection from lenses, and provided that the medium outside of the optical system is homogeneous and nonabsorbing.

The *absorptivity*, a, of any substance is defined as the fraction of incident radiant energy absorbed by it. The *spectral absorptivity*, a_λ, refers to a portion $d\lambda$ of the spectrum as above. A body that has an absorptivity of 1 is known as a *blackbody*. The *emissivity*, e, of any substance is defined as the ratio of the brightness of the substance to the brightness of a blackbody at the same temperature. The *spectral emissivity* e_λ is defined correspondingly.

For a thermal radiator of any kind and for any wave-length the relation between emissivity and absorptivity is given by Kirchhoff's law:

$$\frac{B_\lambda(nb)}{B_\lambda(b)} = e_\lambda = a_\lambda, \qquad (3)$$

where nb and b refer to nonblack and blackbodies, respectively.

A blackbody obeys Lambert's law, that is the brightness B or B_λ is independent of θ. It is a function of temperature alone, according to Planck's radiation law:

$$B_{\lambda(b)} = c_1 \lambda^{-5} \frac{1}{e^{c_2/\lambda T} - 1}, \qquad (4)$$

where $c_1 = c^2 h = 1.40 \times 10^{-12}$ cal. cm^2 sec.$^{-1}$ (c is the velocity of light and h is Planck's constant), and $c_2 = ch/k = 1.433$ cm deg. (k is Boltzmann's constant), and T is expressed in °K.

For short wave-lengths and throughout the visible up to about 0.7μ and for temperatures up to about 3500°K, $e^{c_2/\lambda T} \gg 1$ and Eq. (4) transforms to

$$B_{\lambda(b)} = c_1 \lambda^{-5} e^{-c_2/\lambda T}, \qquad (5)$$

known as Wien's radiation equation.

The line-reversal method rests on the following principle: If a blackbody is placed behind a flame colored, for example, with sodium (which emits the yellow D-doublet, $\lambda = 0.5890 - 6\mu$), and a spectroscope is sighted through the flame onto the blackbody, there will be some temperature of the latter at which its brightness in the spectral region of the D lines equals the brightness of the light transmitted in this region through the flame plus the brightness of the D lines from the flame itself. At this temperature,

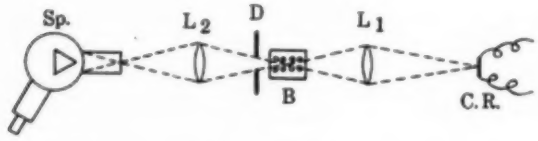

FIG. 1. Diagrammatic sketch of line-reversal apparatus.

therefore, only a continuous spectrum of the blackbody is visible in the spectroscope. At a lower temperature of the blackbody the sodium lines appear bright by contrast against the continuous spectrum. At higher temperatures this contrast reverses itself, the sodium lines appearing dark against the continuous spectrum. At the temperature at which this reversal takes place the following relation applies, if no light is reflected from the flame:

$$B_{D(f)} + B_{D(b)}(1 - a_{D(f)}) = B_{D(b)}, \qquad (6)$$

where the subscript D represents the wavelengths of the D lines and f refers to the flame. Equation (6) can be transformed to

$$\frac{B_{D(f)}}{B_{D(b)}} = a_{D(f)}. \qquad (7)$$

This equation is of the form of Kirchhoff's law (Eq. (3)); and if proof can be obtained of the thermal character of the sodium radiation the temperature of the flame is identical with the reversal temperature.

The metal is usually introduced into the flame as a salt. The salt vaporizes and dissociates into metal atoms and other products. For the measurement of the experimental flame temperature as defined in Section 2 it is not necessary for the salt to vaporize completely or for dissociation equilibrium of the salt to be established. It is only necessary that activation and deactivation of the metal atoms by collisions with other molecules be rapid enough to maintain the equilibrium concentrations of atoms in the electronic quantum states involved in the absorption and emission of the spectral line.

b. Experimental Technique

Figure 1 shows a diagrammatic sketch of the line-reversal apparatus as used on stationary flames. The image of a continuous light source (the comparison radiator, CR) is focused onto a portion of the flame above burner B by means of lens L_1. Diaphragm D defines the beam of light from the flame and comparison radiator which is brought to a focus on the slit of spectroscope S_p by lens L_2, the composite image completely covering the slit. In practice it is not necessary to use a blackbody as comparison radiator; instead, a light source calibrated against a blackbody in the spectral range under consideration may be used. A convenient comparison radiator is a tungsten band lamp, the brightness of whose central portion can be determined as a function of the electric power input. The calibration can be made with an optical pyrometer which itself has been calibrated against a blackbody. The ordinary optical pyrometer utilizes only red brightness by use of a red filter, $\lambda = 0.665\mu$, but the calibration can be extended to other parts of the tungsten spectrum by using spectral emissivity data[6] and Eqs. (3) and (5). Other comparison radiators that have been used are a carbon filament lamp,[5] a Nernst lamp,[7,8] and for very high temperatures a tungsten arc[9] and carbon arc[10] with a rotating sector or absorption glass for diminishing the brightness. If lens L_1 is used between the comparison radiator and the flame, a correction for absorption and reflection due to the lens must be made.[11]

The metal may be introduced into the flame[12] either as a spray of a solution of the salt or as a dry dust. The latter may be introduced directly into the flowing gas by mechanical means or by passage of a spark or arc between salt electrodes containing a metal core[13] or between electrodes immersed in powdered salt. In some investigations a piece of salt was placed on the grid of the burner and was vaporized by the

heat of the flame.[8] The latter method permits coloring of a narrow portion of the flame. It can be accomplished by the spray or dust method if the salt is introduced with a portion of the gas stream passing through a separate smaller tube placed within the burner.

Modifications of the technique of observing the reversal point have been proposed[12] utilizing the contrast effects afforded by uneven brightness along the observed portion of the tungsten strip.

c. Validity of the Method

There is no instance in the literature in which the gas law parameters have been determined simultaneously with the line-reversal temperature. Therefore, within the definition of experimental flame temperature (Section 2) the line-reversal method has never been tested. With Bunsen burners this could be done in principle by measuring the refraction of the gas stream on passing through the boundary of the inner cone using the relationship[14]

$$\frac{\rho_u}{\rho_b} = \frac{\tan \beta}{\tan \alpha}, \tag{8}$$

where ρ_u and ρ_b are the densities of the unburned and burned gases, respectively, α the angle at which the gas stream enters and β the angle at which it leaves the reaction zone. Accurate measurements of β are very difficult.

There is, however, a wealth of other material which has established the validity of the line-reversal method. Using a large Méker burner and coal gas-air mixtures, Bauer[7] found identical reversal temperatures with a number of different salts of sodium and salts of other metals with characteristic line emissions in all parts of the visible spectrum. It does not seem possible to interpret this result in any other way than that statistical equilibrium is established in all cases, either completely or at least between the electronic degrees of freedom of the metal atoms and the translational degrees of freedom of the gas. Since the mixture compositions were not known well enough to permit comparison between the theoretical calculated temperatures and the reversal temperatures, no estimate can be made of the extent to which equilibrium was attained in these experiments. Kohn[8] confirmed Bauer's result of the reversal temperature on the nature of the salt, using again a Méker burner and coal gas-air mixtures of unknown composition. Furthermore, Kohn compared the reversal temperature with the temperature of a wire immersed in the flame and compensated electrically for radiation using a procedure described by Schmidt.[15] A wire, inserted in a flame, emits radiation in a continuous spectrum for which the flame is essentially transparent; it reaches a temperature, lower than that of the gas, at which the flow of energy from the gas to the wire equals the energy radiated from the wire. The wire is now heated by an electric current to a temperature at which there is no further flow of energy from the gas to the wire. The exact amount of current can be determined from knowledge of the radiated energy per unit length of wire as a function of the wire temperature and increasing the wire temperature in the flame until the electric power input equals the radiant energy. The temperature so determined was found to be identical with the line-reversal temperature measured in the neighborhood of the wire. Thus, the same equilibrium exists between the gas and the solid metal as between the gas and the vaporized metal atoms.

Calculation of theoretical flame temperatures for known mixtures is complicated by heat losses to the burner grid and also to the surroundings by radiation and intermixing. In the case of excess fuel, secondary combustion occurs in the outer parts of the flame. There exists, however, a zone of considerable height and width above the grid in which the temperature is quite uniform and in which, therefore, the disturbance due to contact with the atmosphere is negligible, and only losses to the grid and by radiation are important. Reversal temperatures in this zone of Méker flames of known coal gas-air composition and varying flow velocities of the gas were determined by Minkowski, Müller and Weber-Schäfer.[16] Comparison of their values with the theoretical flame temperatures calculated for adiabatic combustion shows that for sufficiently high flow velocity the reversal temperature exceeds the theoretical temperature (see Fig. 2).* In

* Two limiting curves for dry and saturated gases were calculated since the water vapor content was not known.

view of Bauer's and Kohn's results establishing the validity of the line-reversal method, this indicates the existence of excitation lag in the flame gas similar to that found in explosion experiments described in Section 3. Figure 2 also

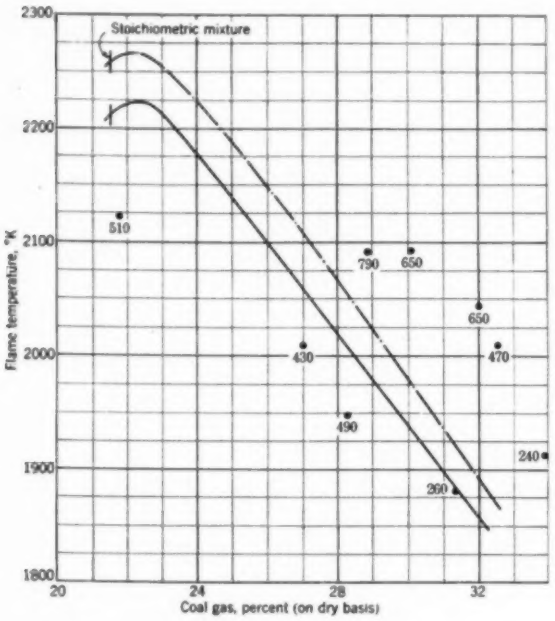

FIG. 2. Comparison of theoretical flame temperatures of coal gas-air mixtures with experimental flame temperatures determined by the line-reversal method. — · — theoretical curve, dry mixtures. ——— theoretical curve, moist mixtures. ● sodium line-reversal flame temperatures with gas velocity in centimeters per second (Minkowski, *et al.*).

shows that the gas velocity required for the reversal temperature to transcend the theoretical temperature becomes larger toward stoichiometric mixtures. This is believed to be in part a consequence of the higher burning velocity of mixtures nearer the stoichiometric because the higher the burning velocity the closer the flame burns to the grid for a given flow velocity and the greater the heat loss. Part of the effect must also be attributed to the higher flame temperatures of such mixtures causing more rapid heat transfer.

Reversal temperature measurements by Kaveler and Lewis[13] on slow burning natural gas-air flames agree very closely with the theoretical temperatures for adiabatic combustion (Fig. 3). Only in the neighborhood of the stoichiometric mixture do the reversal temperatures fall somewhat below the theoretical curve which may be explained in the same way, namely, greater heat loss to the grid for higher burning velocities. If oxygen is substituted for the atmospheric nitrogen in lean mixtures the reversal temperatures are, on the average, somewhat above the theoretical curve (Fig. 4) which is another indication of excitation lag, it being known from explosion experiments that this effect is considerably larger for oxygen than for nitrogen.

In all the investigations mentioned the experimenters were careful to color only the portion of the flame being investigated. If the entire flame is colored the reversal temperature should lie between values for the gas at the center and the gas at the boundary. The latter is cooler than the former in lean mixtures, and hotter, owing to secondary combustion, in rich mixtures. Some early work of Kurlbaum and Schulze[17] which seemed to indicate a dependence on the nature of the salt was shown by Bauer[7] to be in error because of the use of totally colored flames.

In flames of organic fuels the reaction zone is colored blue or green (Swann bands) depending on the mixture composition. This emission is due to C−H or C−C (Swann bands) radicals, respectively. Since these radicals are formed as intermediates in the combustion reaction and probably are excited in the act of formation, it might be expected that their electronic quantum states are not in statistical equilibrium. This is confirmed by observations of Bauer[7] who applied a modified line reversal method to these bands and obtained temperatures, obviously fictitious, which were many hundreds of degrees higher than the possible maximum temperature of the flame. This result has been confirmed independently by Tawde and Patel.[18]

5. Determination of Flame Temperature by Wires and Thermocouples

If a wire or thermocouple is inserted in a flame for thermometric purposes allowance must be made for the temperature difference between wire and gas due to radiation (see Section 4c). This may be done in two ways: (1) By using a series of progressively thinner wires and extrapolating the measured wire temperatures to zero thickness. (2) By compensating the radiation by means of electrical heating. The latter method requires determination of the energy radiated from the wire per unit length and time as a

function of its temperature. This may be done either by measuring the radiation with a thermopile for a series of pyrometrically determined wire temperatures[15] (these measurements may be performed with the wire in any transparent medium, such as the open atmosphere*), or by measuring the electric power input for a series of pyrometrically determined temperatures with the wire placed in a high vacuum so that conduction and convection losses are eliminated.[9]

In the various suction pyrometers[19] used in furnace work the thermocouple is enclosed in a tube through which the furnace gas is passed rapidly enough to bring the walls of the tube to the temperature of the gas. There is thus no radiation loss from the thermocouple to the colder furnace walls. Sometimes the walls of the tube are heated electrically with the current so adjusted that the thermocouple reading remains the same whether the gas is flowing or not.

6. *Determination of Flame Temperature by the Measurement of Brightness and Absorptivity in the Infra-Red*

The temperature of a thermal radiator can be determined by direct measurement of its brightness and absorptivity in some spectral

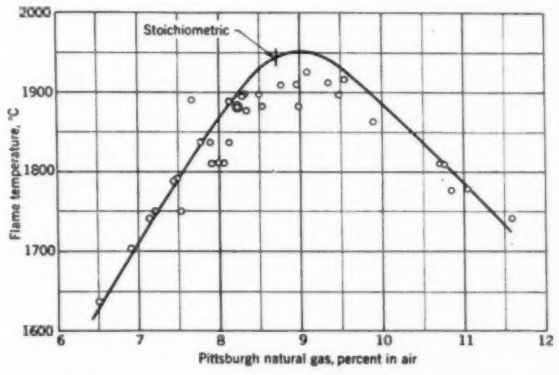

FIG. 3. Highest flame temperatures of Pittsburgh natural gas-air mixtures observed in center of Méker burner flame by sodium line-reversal method. ——— theoretical flame temperatures. ○ observed flame temperatures (Kaveler and Lewis).

range. The relation between these quantities is given by Eqs. (3) and (4). Such measurements were made by Schmidt[15] for wave-lengths between 2.7μ and 4.4μ (bands of H_2O and CO_2)

* Convection and conduction losses do not affect these measurements as has sometimes been erroneously supposed.

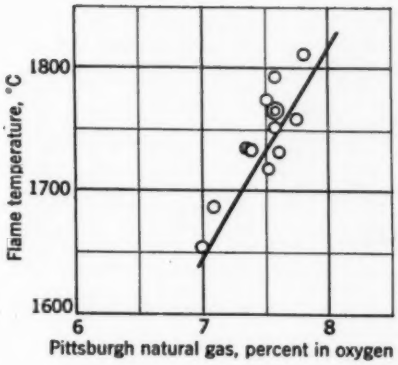

FIG. 4. Highest flame temperatures of Pittsburgh natural gas-oxygen mixtures observed in center of Méker burner flame by sodium line-reversal method. ——— theoretical flame temperatures. ○ observed flame temperatures (Kaveler and Lewis).

and by Bauer[7] for wave-lengths in the region of 25μ (residual rays of fluorite). Both investigators used large Méker burners and coal gas-air mixtures. Schmidt also measured the temperature of the flame by a wire in the manner described above and found fairly good agreement between the temperatures obtained by both methods. Bauer found similar agreement between his measured infra-red temperature and the line-reversal temperature. It is not easy to appreciate the significance of these experiments because infra-red absorption and emission take place throughout the entire depth of the flame on which the instrument is sighted and it is not possible to single out a narrow zone as in the line-reversal and wire methods. Thus, the temperature obtained by the infra-red method should be intermediate between extreme values existing in the flame, as would be the case with the line-reversal method if totally colored flames were used.

7. *Measurement of Temperature and Emissivity of Soot-Forming Luminous Flames*

The slowness of the combustion process in soot-forming, luminous flames of the pre-mixed type with rich mixtures or of the diffusion type insures the absence of any appreciable excitation lag effect, particularly in view of the experience of Kaveler and Lewis[13] with natural gas-air mixtures burning relatively much faster. Thus, the luminous flame has a temperature corresponding to the definition of the theoretical flame temperature—it is a thermal radiator, the bulk

of the radiation being emitted by the soot particles as a continuous spectrum. The soot particles, being cooled by radiation more strongly than the surrounding gas, are at a somewhat lower temperature than the latter. On the basis of data on particle size and heat transfer of solid bodies in gaseous media, Schack[20] has estimated that the temperature difference between the soot particles and the gas should be substantially less than 1°C at usual flame temperatures.

For measuring the temperature of a luminous but not opaque flame Kurlbaum[21] proposed a method similar to the line-reversal method. An optical pyrometer is sighted on a blackbody with and without the flame between them. The temperature of the blackbody is adjusted until its brightness, as seen through the pyrometer, is the same as that observed with the flame interposed. Equation (6) applies which means that both flame and blackbody are at the same temperature, given by the pyrometer reading. Other comparison radiators may be substituted for the blackbody. This method is not easily applicable to industrial furnaces.

Since the presence of soot particles greatly increases the heat transfer by radiation in furnaces much thought has been given to the determination of emissivity of luminous flames from temperature measurements. Schack,[20] after reviewing the data on light absorption of soots from various sources, came to the conclusion that the spectral absorptivity of the flame can be represented by the absorption law for homogeneous absorbing media, namely

$$a_\lambda = 1 - e^{-k_\lambda L} \quad (= e_\lambda, \text{ see Eq. (3)}) \tag{9}$$

where L is the thickness of the absorbing layer and k_λ is the absorption coefficient which, over a limited range of wave-lengths can be represented by the equation

$$k_\lambda = \frac{k}{\lambda^\alpha}, \tag{10}$$

where k and α are constants. Introducing the spectral *brightness temperature* T_λ of the flame, which is the temperature of a blackbody of equal spectral brightness, one obtains from Eqs. (3) and (5)

$$\frac{1}{T} - \frac{1}{T_\lambda} = \frac{\lambda}{C_2} \ln e_\lambda, \tag{11}$$

where T is the true temperature of the flame. If T_λ is measured for a given wave-length and T is determined independently, then from Eqs. (9) and (11) the absorption strength $k_\lambda L$ may be calculated; and since values of α are known over the entire spectral range, e_λ is also known as a function of the wave-length. The desired quantity, the total emissivity of the flame, can then be calculated from Kirchhoff's law for total brightness,

$$e = \frac{\int_0^\infty e_\lambda B_{\lambda(b)} d\lambda}{\int_0^\infty B_{\lambda(b)} d\lambda}, \tag{12}$$

$B_{\lambda(b)}$ being given as a function of λ by the Planck equation (4).

Schack suggested measuring the brightness with an optical pyrometer and the true temperature by some other method such as a suction

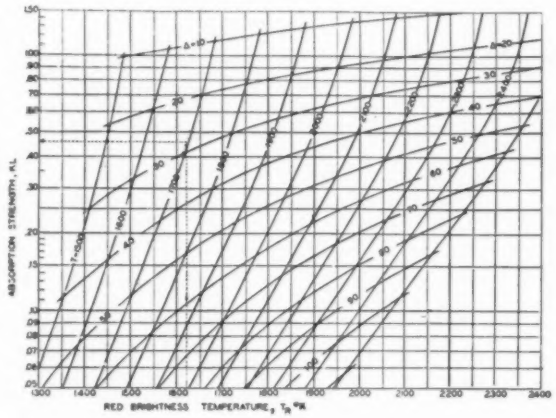

FIG. 5. True temperature and absorption strength of luminous flames as functions of red and green brightness temperatures (Hottel and Broughton).

thermometer. But, as he himself pointed out, the latter method does not allow a precise determination of the usually small difference between T_λ and T, mainly because of the use of two entirely different types of instruments. Hottel and Broughton[22] overcame this difficulty by employing the optical pyrometer exclusively and determining T_λ in two spectral regions, the red and green. Two equations of the type of 11 may now be written with $T_\lambda = T_{\text{Red}}$ and T_{Green}. Hence, T can be eliminated, otherwise the procedure for calculating e remains as before. Hottel and Broughton made further studies of the best values of α to be used. They are $\alpha = 1.39$ up to

$\lambda=0.8\mu$ and $\alpha=0.95$ from $\lambda=0.8\mu$ to 10μ. To eliminate the tedious calculations Hottel and Broughton constructed two graphs (Figs. 5 and 6) from which the true temperature and total emissivity may be read knowing T_R and T_G. From the value of T_R on the abscissa of Fig. 5 one goes vertically to the proper value of (T_G-T_R), then reads the true temperature T by interpolation on the semivertical lines and kL on the ordinate. With this value of kL, e is read from Fig. 6 for any true flame temperature.

Another method adapted to industrial work, namely color pyrometry,[23] makes use of the fact that for many nonblack radiators (so-called gray bodies) the ratio of the spectral brightness for two wave-lengths is about the same as for a blackbody. In its simplest form the color pyrometer consists of a bichromatic wedge-shaped light filter that transmits only red and green. The coefficients of extinction of the two colors differ; as the thickness of the wedge is increased green is absorbed more completely than red. When a radiating body is observed through this type of filter it appears green when viewed through the thin end and red through the thick end. At a certain point in the wedge these two colors, being complementary, merge into white. The position of this point in the wedge depends on the ratio of the red and green brightnesses of the radiating body, i.e., on its temperature, and the length of the wedge can thus be calibrated in terms of temperature. Other more elaborate instruments have been designed with compensating devices for nongray bodies and for overcoming physiological errors.

8. Concluding Remarks

Experimental flame temperatures significantly higher than theoretical temperatures have been observed only in fast flames such as hydrogen and coal gas flames. In furnace flames there appears to be no reason to expect appreciable deviations from statistical equilibrium except perhaps near the orifice in pre-mixed flames—disturbances such as heat transfer are too slow to affect the statistical equilibrium. Thus, there is no anomaly to be dealt with and temperature measurements should give the true flame temperature that corresponds to the theoretical flame temperature as defined in Section 2.

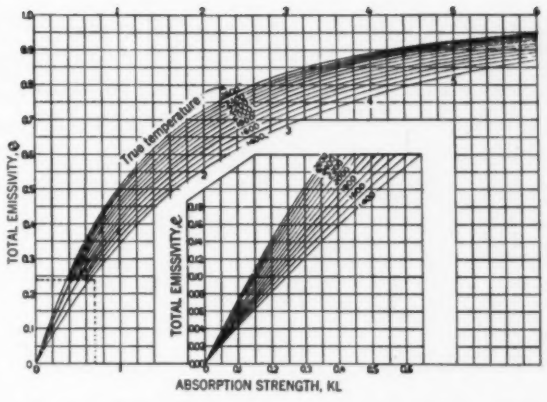

FIG. 6. Total emissivity of luminous flame from its true temperature and absorption strength (Hottel and Broughton).

In internal combustion engines where the flame is greatly speeded up by turbulence, appreciable excitation lag may occur, but owing to the complexity of the process there seems to be no practical way at present to determine its contribution to the pressures developed. Rassweiler and Withrow[24] determined a temperature of 2060°C at the firing end of an Otto cycle engine using the line reversal method. This temperature was calculated later by Hottel and Eberhardt[25] to be 2071°C on the basis of adiabatic combustion. The measured temperature is undoubtedly lowered by cooler gas layers near the observation window.

Flame temperatures of various combustibles and the change of flame temperature with the air-fuel ratio can be compared from calculations on the basis of adiabatic combustion. These calculations are tedious and have been done with accurate data only for a few cases.[1] In most instances where less accurate older data have been used the results are in error by not more than 50° and may still be used as a basis of comparison of various mixtures. Lacking calculated values, the large amount of data of line-reversal temperatures may prove useful although these data were, as a rule, obtained with totally colored flames. Such line-reversal temperatures are uniformly lower than the theoretical temperatures by amounts ranging from 30 to 80°C. Extensive tables have been compiled by Lewis and von Elbe.[26]

In gases where statistical equilibrium is very strongly disturbed, such as in discharge

tubes and in the hydrogen torch, the term temperature loses much of its practical significance although it may still be a definable quantity on the basis of the translational energy of the gas. Pirani and Rompe[27] have proposed to denote the degree of freedom or the molecular state that primarily acquires the energy added to the system as "energy flow trap." For ordinary flame gases this term does not seem to be usefully applicable.

9. *Summary*

The discussion is confined to flames produced incident to the use of fuels for heating and generation of power. The theoretical flame temperature corresponding to complete statistical equilibrium in the burned gas is distinguished from the experimental flame temperature measured by the gas law equation and corresponding to equilibrium in the translational degrees of freedom. Experiments on fast flames in closed vessels show that the latter may be higher than the former due to excitation lag in the internal, presumably vibrational, degrees of freedom.

The theory and technique of the line-reversal method are described and the experimental evidence is interpreted as indicating that the method yields the experimental flame temperature as defined above. The technique of measuring flame temperatures by wires and thermocouples is described. In measurements of flame temperatures by infra-red radiation temperature variation within the flame is a disturbing factor.

Soot-forming luminous flames may be regarded to be in complete statistical equilibrium, the temperature difference between soot particles and the surrounding gas being negligible. Methods of determining the temperature and emissivity of such flames are described. In industrial furnaces the differences between the experimental and theoretical temperatures should be negligible and there is thus no reason to question the existence of a true temperature. In internal combustion engines excitation lag is likely to exist but no experimental confirmation is available. The term "energy flow trap" does not seem to have useful application in technical combustion processes.

Bibliography

1. B. Lewis and G. von Elbe, *Combustion, Flames and Explosions of Gases* (Cambridge University Press, 1938).
2. See, for example, H. O. Kneser and V. O. Knudson, Ann. d. Physik **21**, 682 (1935), and other references mentioned there.
3. B. Lewis and G. von Elbe, J. Chem. Phys. **7**, 197 (1939).
4. B. V. Korvin-Kroukovsky, J. Frank. Inst. **221**, 99 (1939).
5. Ch. Féry, Comptes rendus **137**, 909 (1903).
6. W. E. Forsythe and A. G. Worthing, Astrophys. J. **61**, 140 (1925).
7. E. Bauer, *Recherches sur le rayonnement*, Théses (Gauthier-Villars, Paris, 1912).
8. H. Kohn, Ann. d. Physik **44**, 749 (1914).
9. E. Griffiths and J. H. Awbery, Proc. Roy. Soc. **A123**, 401 (1929).
10. F. Henning and C. Tingwaldt, Zeits. f. Physik **48**, 805 (1928), H. H. Lurie and G. W. Sherman, Ind. Eng. Chem. **25**, 404 (1933).
11. For details see G. W. Jones, B. Lewis, J. B. Friauf and G. St. J. Perrott, J. Am. Chem. Soc. **53**, 869 (1931).
12. Cf. G. Ribaud, Y. Laure and H. Gandry, Inst. of Fuel, Symposium on Gas Temperature Measurement, Vol. 12, March, 1939, pp. 18–30.
13. H. H. Kaveler and B. Lewis, Chem. Rev. **21**, 421 (1937).
14. Gouy, Ann. Chim. Phys. (5) **18**, 27 (1879); cf. reference 1.
15. H. Schmidt, Ann. d. Physik **29**, 1027 (1909).
16. R. Minkowski, H. G. Müller and M. Weber-Schäfer, Zeits. f. Physik **94**, 145 (1935).
17. F. Kurlbaum and G. Schulze, Verh. d. D. Phys. Ges. **5**, 427 (1903).
18. N. R. Tawde and J. M. Patel, J. Univ. of Bombay **6**, 29 (1937).
19. Cf. Inst. of Fuel, Symposium on Gas Temperature Measurement, Vol. 12, March, 1939.
20. A. Schack, Zeits. f. tech. Physik **6**, 530 (1925).
21. F. Kurlbaum, Physik. Zeits. **3**, 187 (1902).
22. H. C. Hottel, and F. P. Broughton, Ind. Eng. Chem. (Anal. Ed.) **4**, 166 (1932).
23. G. Naeser, Inst. of Fuel, Symposium on Gas Temperature Measurement, Vol. 12, March, 1939, p. 38; W. Bowen, *ibid.*, p. 75.
24. G. Rassweiler and L. Withrow, J. Soc. Aut. Eng. **36**, 125 (1935).
25. H. C. Hottel and J. E. Eberhardt, Chem. Rev. **21**, 439 (1937).
26. Reference 1, pp. 398–401.
27. M. Pirani and R. Rompe, Trans. Electrochem. Soc. **69**, 417 (1936); cf. J. G. Bennett and M. Pirani, Inst. of Fuel, Symposium on Gas Temperature Measurement, Vol. 12, March, 1939, p. 1.

Resumés of Recent Research

Thermal Conductivity of Metals From the standpoint of modern theory, the expression for thermal conductivity of a metal should contain two additive terms, one due to the lattice and one due to the electron conductivity. A. H. Wilson[1] gives the equation as

$$k=\frac{1}{3}\rho C l u+\frac{\pi^2}{3}\cdot\frac{n\tau k_0^2 T}{m}. \qquad (1)$$

k is the thermal conductivity; ρ, the density; C, the atomic heat; l, the electron mean free path in the lattice; u, the velocity of elastic waves (sound) in the lattice; n, the number of free electrons per unit volume; τ, the "relaxation time" (average time between collisions); k_0, the molecular gas constant; m, the mass of the electron; T, the absolute temperature.

If we write the equation as

$$\frac{k}{\rho C}=\frac{1}{3}lu+\frac{\pi^2}{3}\frac{n\tau k_0^2 T}{m\rho C} \qquad (2)$$

it is in the form

$$\frac{k}{\rho C}=K\frac{1}{T}+K'. \qquad (3)$$

This assumes that $\tau \propto T^{-1}$ and $lu \propto T^{-1}$ and that ρ and C compensate as to their temperature effects.

The equation in this latter form is experimentally verified by data on tin, lead and zinc.[2] Values of $k/\rho C$, plotted as ordinates against $1/T$ as abscissa, give straight lines with intercepts on the y axis and *these intercepts turn out to be the values of $k/\rho C$ for the molten state.*

The conductivity for the molten state includes the residual atomic conductivity as well as that due to electrons. The conductivity of an insulating liquid is very small (1 percent, or less, of that of a conductor). Hence the last term on the right is, very likely, almost entirely electron conductivity. The temperature effect for the solid is seen to be entirely, or nearly entirely, due to the elastic lattice. The data indicate little or no temperature effect in the liquid state.

Thermal conductivity measurements on other metals offer much greater difficulty than was the case for those here reported, which are fairly low melting point metals. However, from the law indicated, one may venture to predict the thermal conductivity for the molten state for any metal provided enough data are available on the solid state to establish the straight line and obtain the intercept.

Measurements were not carried below the temperature of liquid nitrogen (−195°C) and it is not expected that these relations should hold at extremely low temperatures.

Young's Modulus of Beta-Brass Crystals The marked changes in the physical properties of certain ordered alloys as they go through the order-disorder transition have been measured extensively for polycrystalline material, but little work has been done with single crystals. Recently,[1] however, the change in Young's modulus of seven single crystals of beta-brass, an approximately equimixture of copper and zinc has been measured as a function of temperature. The method used was that of the composite piezoelectric oscillator. From such measurements it is possible to obtain Young's modulus for any direction in the crystal lattice. Plots of the reciprocal of Young's modulus in the three principal directions, [100], [110], and [111], (cube edge, face-diagonal, and body-diagonal, respectively), show that the effect of disorder is mainly felt in the first two directions, while in the third direction the elasticity shows an approximately linear increase with increasing temperature. This is very surprising in view of the fact that in almost every other known material just the reverse is true. In the [111] direction the behavior of Young's modulus is like that for an isotropic solid, while in the [110] direction there is almost zero change in $1/E$. An unusual degree of anisotropy in Young's modulus at room temperature, as shown by the large ratio, 8.2, of maximum to minimum modulus in the [111] and [100] directions, was noted, and this may account for the peculiar temperature dependence of Young's modulus in different directions in the crystal.

[1] A. H. Wilson, *Semiconductors and Metals* (Macmillan, New York, 1939).

[2] This note is a resume of papers by C. C. Bidwell in Phys. Rev. **56**, 594–598 (1939); **58**, 561–564 (1940). A precise method is there described for making thermal conductivity measurements at high temperatures, applicable to either solid or molten metals.

[1] J. Rinehart, Phys. Rev. **58**, 365 (1940).

Here and There

Increased Facilities for Optical Work

In order to provide facilities for the production of optical instruments and optical parts required by the National Defense Program, the Spencer Lens Company, Scientific Instrument Division of American Optical Company, has let a contract to The Gillmore-Carmichael-Olson Company for the construction of additional buildings at the Eggert Road site, Buffalo, New York, Mr. B. H. Witherspoon, president of the Company, announces. One unit of approximately the same size as the present Mechanical Parts Plant, completed last summer, will house certain prism and lens manufacture. A connecting unit two and three stories high will be utilized for the assembly of special contract work. A third unit will provide expansion for the mechanical parts operations. It is planned to have the new unit in operation not later than February 1, 1941.

★

National Defense Products

General Electric leads American industry in variety of products being made for the national defense program, according to a statement made by Philip D. Reed, General Electric Board Chairman, in a recent address before the Chamber of Commerce and the Junior Chamber of Commerce of San Francisco. "A significant portion of the General Electric Company's productive capacity will be fully occupied with rearmament work," Mr. Reed pointed out. He also stated, however, that he believed the Company's normal output of useful goods can be maintained and in certain departments substantially increased. The continuation on the part of industry of the production of useful goods is important, in Mr. Reed's opinion, if inflation is to be prevented and American standards of living preserved.

★

National Chemical Exposition

New discoveries and developments in the service of chemistry and its application and progress in many fields of activity will be discussed by foremost authorities in America at an Industrial Chemical Conference, which will be a feature of the National Chemical Exposition to be held December 11 through 15 at the Stevens Hotel in Chicago.

"We have arranged for this Industrial Chemical Conference an excellent program of papers in the nature of symposia on 'Newer Developments in Chemistry and Chemical Engineering,'" said Dr. R. C. Newton, chairman of the show committee. "The program is timed to afford those who wish to hear the talks in which they are interested ample opportunity also to view the show." Technical sessions for this conference have been arranged for Thursday afternoon and evening, December 12; Friday forenoon, December 13, and Saturday afternoon, December 14.

New Calcite Source Discovered

A new source of calcite, or Iceland spar, a valuable optical mineral heretofore imported from abroad, was revealed recently when officials of the Bausch & Lomb Optical Company announced they had contracted for the output of a new mine in the San Pedro mountains, northwest of Santa Fe, New Mexico. The discovery by a Mexican prospector of the new source of supply and the interest of E. M. Stanton, a Chicago optometrist, led to a subsidy by Bausch & Lomb through which operations have been carried on.

The scarcity of optical calcite has caused a world-wide search for many years, since the mineral is essential in the construction of all polarizing instruments. With the flooding of the Iceland mine at Helgustadir during the World War, this source which formerly supplied the world has been unproductive of fine crystals. Meager supplies have come from various countries, the most recent from Spain and South Africa, but the total volume offered for sale has been insignificant for many years.

Officials reported that the new mine had delivered more than five hundred pounds of fine calcite crystals within a period of three months, many of them weighing as high as forty pounds. An analysis of the output of the new mine indicates that the United States now has a supply of calcite of high optical quality which will serve the country for years.

★

Company Expansion Planned

The Westinghouse Electric and Manufacturing Company will spend more than $8,500,000 during the year ending next June, to increase its emergency and peacetime production facilities. The Company's expansion authorization provides some $5,000,000 for machine tools and equipment, in addition to the construction of 15 new buildings in six different states. Another $6,000,000 has been authorized for maintenance of the expanded plant facilities.

Since last June, Westinghouse has completed five buildings; nine are under construction, and another is contemplated. Two structures now nearing completion are a temporary building for production of radio equipment for the Government at the Westinghouse Radio Division in Baltimore, Maryland, and a service plant at Bridgeport, Connecticut. Two additional buildings for Government radio production and a service plant are under construction at Baltimore. Three factory additions and a warehouse are being built at the Westinghouse Merchandising Division, Mansfield, Ohio.

A $500,000 office building at the Westinghouse Steam Division, South Philadelphia, and additional factory space, including a new printing plant, at the Westinghouse Micarta Plant, Trafford, Pennsylvania, are under way. A $300,000 district headquarters and service building has been authorized for Atlanta, Georgia.

University of Maine Faculty Promotions

The following promotions in the Department of Physics at the University of Maine have been made this year:

Professor Clarence E. Bennett, formerly Associate Professor and Department Head, to Professor and Department Head;

Dr. Arthur O. Williams, Jr., from instructor to Assistant Professor;

Mr. Frederick B. Oleson from assistant to part-time instructor.

★

Meteorology

Commander F. W. Reichelderfer, of the U. S. Weather Bureau, has made a statement to the effect that only three institutions in the country now have an advanced meteorological course, and these have each graduated from ten to twenty men a year. Most of the men have been Army and Navy officers sent there by the military service. There have been only about ten to twenty men each year for civilian occupations. This is due to the fact that the opportunity for employment has been limited. However, he states that the new five-day weather forecasting system, initiated recently by the Weather Bureau, is creating a demand for meteorologists.—*Science*

★

Mathematical Biophysics

The table of contents of the December issue of the *Bulletin of Mathematical Biophysics*, published by the University of Chicago Press, includes the following articles:

Some General Theorems on the Motion of Incompressible Viscous Fluids, by G. YOUNG

A Neural Mechanism for Discrimination. III. Visually Perceived Lengths and Distances, by A. S. HOUSEHOLDER

Deformation of Shell Shaped Cellular Aggregates: Application to Gastrulation, by N. RASHEVSKY

Some Considerations on Mathematical Molecular Biophysics, by N. RASHEVSKY

Communications for the editor and manuscripts should be addressed to N. Rashevsky, Editorial Office of the *Bulletin of Mathematical Biophysics*, 5822 Drexel Avenue, Chicago, Illinois.

★

Color Television

From the Columbia Broadcasting System comes an announcement of its laboratory success in developing color television. It is hoped that the manufacture of commercial equipment in this field will be started within the next few months, although, since Columbia is not itself a commercial manufacturer of television apparatus, it is not possible for the Company to say how long it will take for the actual marketing of the necessary devices to be begun.

★

Dr. Hans Bethe, Professor of Physics at Cornell University, has been granted a sabbatical leave from February, 1941, until February, 1942. He will spend the spring semester of 1941 at Columbia University, where he has been invited to lecture.—*Science.*

35,000-Foot Parachute Jump

For the purpose of solving some of the problems of stratosphere flying, a six-and-a-half-mile parachute jump, to be made in the interest of science by amateur Arthur H. Starnes, was being planned when this material went to press. In the laboratories of the Armour Research Foundation of Illinois Institute of Technology, scientists of the University of Chicago and Northwestern University gathered on September 23 to conduct final tests preliminary to the proposed 35,000-foot leap to be undertaken sometime within the two weeks following that date. Unique in the history of science and aviation, the tests simulated conditions of temperature and wind velocities which Starnes was expected to encounter as he hurtled earthward at 200 miles per hour. Fully clothed in jumping regalia, replete with 103 pounds of scientific instruments, Starnes was put through the cold wind tunnel tests.

In addition to the interest of science in the jump planned, it was revealed that much of the data and information obtained thus far through the researches carried on by experts from Chicago and Northwestern Universities will be turned over to the officers of the Army and Navy, whose interest in them is based on the increased importance of parachute troops.

★

Executives Receive Promotions

W. Richison Schofield, formerly chief engineer of Leeds & Northrup Company, Philadelphia, has recently been appointed Director of Engineering. John W. Harsch, Assistant Chief Engineer, has been advanced to Chief Engineer, and Mr. Harsch's former position has been filled by the promotion of John F. Quereau.

★

Calendar of Meetings

October

28–Nov. 2 Conference on Applied Nuclear Physics, Cambridge, Massachusetts

November

11–15 American Petroleum Institute, Chicago, Illinois
15–16 Acoustical Society of America, Chicago, Illinois
22–23 American Physical Society, Chicago, Illinois

December

2– 4 American Institute of Chemical Engineers, New Orleans, Louisiana
2– 7 Highway Research Board of National Research Council, Washington, D. C.
3– 6 American Society of Mechanical Engineers, New York, New York
20–21 American Physical Society, Pasadena, California
26–28 American Physical Society, Philadelphia, Pennsylvania
26–28 Geological Society of America, Austin, Texas
28–30 American Association of Physics Teachers, Philadelphia, Pennsylvania
27–Jan. 2 American Association for the Advancement of Science, Philadelphia, Pennsylvania

February

21–22 Joint meeting, American Physical Society and Optical Society of America, Cambridge, Massachusetts

April

7–11 American Chemical Society, St. Louis, Missouri

May

1– 3 American Physical Society, Washington, D. C.

June

20–21 American Physical Society, Providence, Rhode Island
23–27 American Association for the Advancement of Science, Durham, New Hampshire

Biophysics Fellowship

Union College, Schenectady, New York, made recent announcement of a fellowship in biophysics for 1940–41. Further information may be obtained from President Dixon Rayan Fox, Union College, Schenectady, New York.

Conference on Electrical Insulation

The Conference on Electrical Insulation of the National Research Council (Division of Engineering and Industrial Research) is holding its annual meeting in Washington, D. C., on October 31 and November 1 and 2.

Contributors to This Issue

C. S. Barrett

Charles S. Barrett, since receiving his Ph.D. degree at the University of Chicago in 1928, has been active in research in physical metallurgy and applied x-rays, first at the Naval Research Laboratory and now at Carnegie Institute of Technology in Pittsburgh.

E. A. Walker

Eric A. Walker is Associate Professor of Electrical Engineering at the University of Connecticut. He received his Sc.D. degree from the Harvard Engineering School in 1935. From 1934 to 1940 Dr. Walker was a member of the faculty of Tufts College Engineering School and in 1939 was made chairman of the Department of Electrical Engineering.

H. Ôkubo

H. Ôkubo was appointed Professor of the Mechanical Engineering Department of the Yonezawa Technical College, Yonezawa, Japan, in 1939. In 1929 he was graduated from the Tôhoku Imperial University in Sendai, Japan.

A. Rose

Albert Rose has held, since 1935, the post of Research Engineer in the Research Laboratories, RCA Manufacturing Company, Inc., Harrison, New Jersey. He received the Ph.D. degree in physics at Cornell University, where he was teaching assistant from 1931 to 1934.

D. C. Drucker

Daniel C. Drucker was Research Assistant in Civil Engineering at Columbia University during 1938–39 and University Fellow during 1939–40 when he completed course and thesis requirements for the Ph.D. degree. He is now instructor in mechanics at Cornell University.

A. H. Geisler

Alfred H. Geisler, after receiving his B.S. degree in metallurgy at Carnegie Institute of Technology in 1938, undertook graduate studies and at present holds the Aluminum Company of America Graduate Fellowship at Carnegie Institute of Technology.

The following contributors have received mention in earlier issues of the *Journal of Applied Physics:*

Bernard Lewis, p. 388, Vol. 10, No. 6, 1939.
Guenther von Elbe, p. 388, Vol. 10, No. 6, 1939.
Raymond D. Mindlin, p. 704, Vol. 9, No. 11, 1938.
Morris Muskat, p. 391, Vol. 9, No. 6, 1938.

Contributed Original Research

A Mechanical Model for the Motion of Electrons in a Magnetic Field

ALBERT ROSE
Research Laboratories, RCA Manufacturing Company, Inc., Harrison, New Jersey
(Received June 8, 1940)

A mechanical model in the form of a gyroscope may be made to simulate the path of an electron in a uniform magnetic field acted upon by transverse electric fields. In using the model, one employs the following substitutions: The uniform magnetic field is replaced by the spin velocity of the gyroscope, the electric fields are replaced by magnetic fields which give the same field configuration, and the electron is replaced by one pole of a permanent magnet mounted on the axis of the gyroscope. The spin velocity may be arbitrarily chosen for convenient observation. Then, depending upon the value of the spin velocity, the dimensions of the gyroscope, the strength of the permanent magnet and the scale factor used in setting up the model, the strength of the magnetic field in the model is adjusted to correspond to the strength of the electric field in the actual case. The path described by the magnetic pole, under these conditions, corresponds to the actual path of the electron. Since the error involved in identifying the equations of motion of the gyroscope with those of the electron is of the order of θ^2, where θ is the half-angle of the cone through which the spin axis is allowed to move, the range of observations must be restricted accordingly. Some familiar structures for which electron paths have been observed and photographed are deflection plates in a uniform magnetic field, a diode in an axial magnetic field, and a split-anode magnetron. By periodically reversing the current through the field magnets, it is possible to observe the effect of alternating electric fields. In one arrangement, in which the field was alternated in resonance with the revolution of the electron about the magnetic field lines, a path similar to that of charged particles in a cyclotron was obtained.

INTRODUCTION

MECHANICAL analogs of electron motion have been found of value not only as an aid to pedagogy but also as an aid to original investigations in the design of modern electron tubes. The use of small balls rolling on a rubber membrane to simulate the motion of electrons in a two-dimensional electrostatic field is a well-known example. While this model has been widely used, similar models for electron motion in the presence of a magnetic field either have not been proposed or have not been convenient enough for ready application.[1] This paper will describe a simple model for the motion of electrons acted upon by a two-dimensional electric field in a plane normal to a uniform axial magnetic field. The essential part of this model and that which traces the electron paths is a gyroscope mounted with its axis in the direction of the magnetic field.[2] The first part of the paper will compare the equations of motion of an electron, in the electric and magnetic fields mentioned above, with the equations of motion of the end of the axis of the gyroscope acted upon by forces normal to its axis. From this comparison, the approximations involved in using the model will be set forth as well as the quantitative relations between the constants in the two sets of equations. The second part of the paper will describe the application of the model to some familiar types of electron motion and will include photographs of the electron paths as traced by the gyroscope.

ANALYSIS OF THE MODEL

In the cylindrical-coordinate system r, ϕ, z of Fig. 1, let H be a uniform magnetic field in the

[1] A mechanical model for electron motion in axially symmetric magnetic fields is described by E. Bruche and A. Recknagel (Zeits. f. tech. Physik **17**, 126–134, 1936). This form requires a separate construction of the model for each set of initial conditions.

[2] It has come to the writer's attention, since this paper was written, that the similarity between the force on an electron due to its motion transverse to a magnetic field, and the force on a gyroscope due to the angular velocity of its axis was suggested in 1933 by Professor E. C. Kemble. (See William F. Osgood, *Mechanics* (Macmillan, 1937), p. 234.)

Electron Equations of Motion	Gyroscope Equations of Motion
	$(\theta^2 \ll 1)$
$\ddot{r}-r\dot{\phi}^2=-r\dot{\phi}H\frac{e}{m}-E_r\frac{e}{m}$	$\ddot{r}-r\dot{\phi}^2=-r\dot{\phi}\dot{\Psi}\frac{C}{A}+F_r\frac{L^2}{A}$
$r\ddot{\phi}+2\dot{r}\dot{\phi}=\dot{r}H\frac{e}{m}-E_\phi\frac{e}{m}$	$r\ddot{\phi}+2\dot{r}\dot{\phi}=\dot{r}\dot{\Psi}\frac{C}{A}+F_\phi\frac{L^2}{A}$
$\ddot{z}=0$	$\ddot{\Psi}=0.$

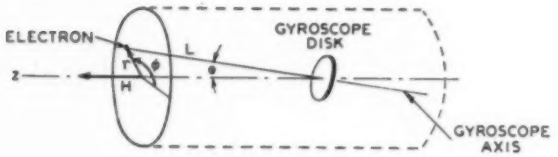

$$H\frac{e}{m}\rightarrow\dot{\Psi}\frac{C}{A}$$

$$E_r\frac{e}{m}\rightarrow F_r\frac{L^2}{A}$$

$$E_\phi\frac{e}{m}\rightarrow F_\phi\frac{L^2}{A}$$

FIG. 1. Equations of motion of an electron in a uniform magnetic field and of the end point of the axis of a gyroscope.

z direction, and let E_r, E_ϕ, E_z be the electric field intensities in the r, ϕ, and z directions. The equations of motion of an electron in this system are

$$\ddot{r}-r\dot{\phi}^2+e/mr\dot{\phi}H=-e/mE_r, \quad (1a)^*$$

$$r\ddot{\phi}+2\dot{r}\dot{\phi}-e/m\dot{r}H=-e/mE_\phi, \quad (1b)$$

$$\ddot{z}=-e/mE_z. \quad (1c)$$

Of these equations, we shall be primarily interested in (1a) and (1b) which describe the motion of the electron in the $r-\phi$ plane, since the application of the model is restricted to this plane. Fortunately, motion of the electron in the z direction is independent both of H and of motion in the r and ϕ directions. The z component of the electron path may be obtained from a knowledge of E_z and may readily be combined with the $r-\phi$ plane projection of the path to give the complete picture.

Corresponding to Eqs. (1a) and (1b) for the electron, we now desire similar equations for the motion of the end point of the gyroscope axis in the same $r-\phi$ plane. The motion of the gyroscope has been treated extensively both in technical journals and in textbooks on mechanics. It will, therefore, suffice to indicate here the method for obtaining the particular form of the equations of motion used in this paper. Lagrange's equations for the general case of a rotating rigid body fixed at its center of gravity are

$$\frac{\partial}{\partial t}\left(\frac{\partial T}{\partial\dot{\theta}}\right)-\frac{\partial T}{\partial\theta}=L_\theta F_\theta, \quad (2a)$$

$$\frac{\partial}{\partial t}\left(\frac{\partial T}{\partial\dot{\phi}}\right)-\frac{\partial T}{\partial\phi}=L_\phi F_\phi, \quad (2b)$$

$$\frac{\partial}{\partial t}\left(\frac{\partial T}{\partial\dot{\psi}}\right)-\frac{\partial T}{\partial\psi}=L_\psi F_\psi. \quad (2c)$$

The coordinate angles θ, ϕ, ψ are the Eulerian angles, two of which, θ and ϕ, are shown in Fig. 1. The third angle, ψ, measures the rotation of the gyroscope disk with respect to the plane formed by the gyroscope axis and the z axis (Fig. 1). F_θ, F_ϕ, F_ψ, are the forces and L_θ, L_ϕ, L_ψ, the moment arms for the three torques. The kinetic energy function, T, is most readily expressed as

$$T=\tfrac{1}{2}(A\omega_1^2+B\omega_2^2+C\omega_3^2), \quad (3)$$

where A, B, C are the principal moments of inertia and ω_1, ω_2, ω_3 are the angular velocities about the three principal axes of inertia. The explicit expression for $\partial T/\partial\dot{\theta}$, and similar terms in Eq. (2), is obtained from

$$\frac{\partial T}{\partial\dot{\theta}}=A\omega_1\frac{\partial\omega_1}{\partial\dot{\theta}}+B\omega_2\frac{\partial\omega_2}{\partial\dot{\theta}}+C\omega_3\frac{\partial\omega_3}{\partial\dot{\theta}}, \text{ etc.} \quad (4)$$

and from the transformation equations:[3]

$$\omega_1=\dot{\theta}\sin\psi-\dot{\phi}\sin\theta\cos\psi, \quad (5a)$$

$$\omega_2=\dot{\theta}\cos\psi+\dot{\phi}\sin\theta\sin\psi, \quad (5b)$$

$$\omega_3=\dot{\psi}+\dot{\phi}\cos\theta. \quad (5c)$$

* Note: the absolute value of "e," the charge on the electron, is used throughout this paper.

[3] See J. H. Jeans, *Theoretical Mechanics* (Ginn and Company, 1907), p. 347.

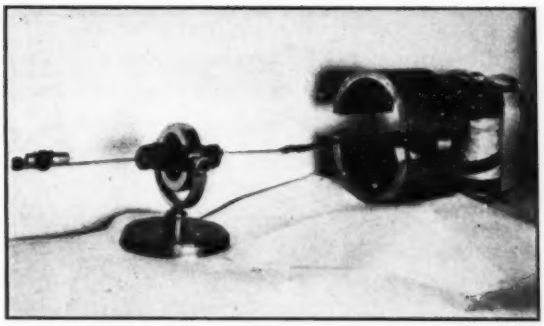

FIG. 2. Gyroscope set up to record the path of an electron in a magnetron.

These equations, together with the fact that if C is the moment of inertia about the gyroscope (or spin) axis A is equal to B by symmetry, allow Eq. (2) to be written as

$$A\ddot{\theta}+C\dot{\psi}\dot{\phi}\sin\theta-(A-C)\dot{\phi}^2\sin\theta\cos\theta=L_\theta F_\theta, \quad (6a)$$

$$A\ddot{\phi}\sin^2\theta-C\dot{\psi}\dot{\theta}\sin\theta+2(A-C)\dot{\phi}\dot{\theta}\sin\theta\cos\theta+C(\dot{\psi}+\ddot{\phi}\cos\theta)\cos\theta=L_\phi F_\phi, \quad (6b)$$

$$C(\ddot{\psi}+\ddot{\phi}\cos\theta-\dot{\phi}\dot{\theta}\sin\theta)=L_\psi F_\psi. \quad (6c)$$

In the ordinary operation of the gyroscope, if one neglects friction, $F_\psi=0$ so that

$$\ddot{\psi}+\ddot{\phi}\cos\theta-\dot{\phi}\dot{\theta}\sin\theta=0 \quad (7)$$

and

$$\dot{\psi}+\dot{\phi}\cos\theta=\text{constant}. \quad (8)$$

From Eq. (8), the constant is equal to the value of $\dot{\psi}$ when $\phi=0$. That is to say, if the gyroscope is given an initial spin velocity and then allowed to move under the influence of forces transverse to the axis, the constant is equal to the initial spin velocity. Let $\dot{\Psi}$ be this spin velocity. Eqs. (7) and (8) with the constant replaced by $\dot{\Psi}$ may be used to rewrite Eq. (6) as

$$\ddot{\theta}-\dot{\phi}^2\sin\theta\cos\theta+C/A\dot{\phi}\dot{\Psi}\sin\theta=\frac{LF_\theta}{A}, \quad (9a)$$

$$\ddot{\phi}\sin\theta+2\dot{\phi}\dot{\theta}\cos\theta-C/A\dot{\theta}\dot{\Psi}=\frac{LF_\phi}{A}, \quad (9b)$$

$$\ddot{\Psi}=0. \quad (9c)$$

On the assumption that the point of application of the forces F_θ and F_ϕ is at the end of the axis of the gyroscope, L_θ and L_ϕ become according to Fig. 1, L and $L\sin\theta$. At this point it is well to emphasize that no approximations have yet been made. Eqs. (9a), (9b), and (9c) are the equations of motion of a rigid body, with its center of gravity fixed and with its spin axis an axis of symmetry, subjected to forces transverse to the spin axis—in brief, the equations of motion of a gyroscope. If, now, θ is restricted to small values such that $\theta^2\ll1$, we can replace $\cos\theta$ by 1 and $\sin\theta$ by r/L where r is the distance the end of the gyroscope axis moves, measured along the arc of its motion, from its origin at the z axis. Since θ is restricted to small values, the "r" defined above may be identified with the r in Fig. 1 used as one coordinate of the electron in the $r-\phi$ plane. With this approximation, (9a) and (9b) may be written in a form to be compared with the electron equations (1a) and (1b), namely

$$\ddot{r}-r\dot{\phi}^2+C/Ar\dot{\phi}\dot{\Psi}=\frac{L^2}{A}F_r, \quad (10a)$$

$$r\ddot{\phi}+2\dot{r}\dot{\phi}-C/A\dot{r}\dot{\Psi}=\frac{L^2}{A}F_\phi. \quad (10b)$$

Comparison of Eqs. (10) and (1) shows first, that the two sets are identical in form and, second, that the following correspondences exist between their parameters:

electron	*gyroscope*	
e/mH	$C/A\dot{\Psi}$,	(11a)
e/mE_r	L^2/AF_r,	(11b)
e/mE_ϕ	L^2/AF_ϕ.	(11c)

The formal identity of the two sets of equations says, immediately, that if a scale model of the force field E_r, E_ϕ is set up so that it acts transverse to the axis of a rotating gyroscope, then the path described by the end point of the gyroscope is, for small values of θ, the path that an electron would describe in that force field and in a uniform magnetic field normal to the plane of the force field. Variations of the spin velocity of the gyroscope or of the magnitude or direction of parts of the force field will alter the path of the gyroscope and allow one to obtain a qualitative understanding of the changes of path that

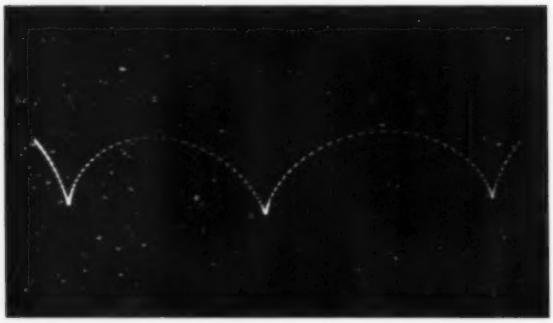

FIG. 3. Cycloidal path of an electron in crossed electric and magnetic fields.

an electron would undergo for similar variations of magnetic and electric fields. This is usually the way in which a model is used. It is, nevertheless, desirable to know also the quantitative relations between the "magnetic" and "electric" fields of the scale model and the actual magnetic and electric fields acting upon the electron. A discussion of these relations follows.

The performance of the model differs from the performance of the electron in two significant respects. First, the model takes longer to describe its path than does the electron. Second, the model is usually constructed to operate on a larger scale. (Since the model represents only one electron, the paths it describes are free from the influence of space charge.) The question is: "Under what conditions will the electron path be unchanged when either (or both) the transit time and the scale factor are changed?" By "unchanged" is meant either "identical" when only the transit time is changed or "differing only by the scale factor" when the scale factor of the electrodes is changed. These conditions may be obtained in the following manner. Let the time scale in Eq. (1a) be changed from t to t/k where k is an arbitrary constant. Then, He/m which has the dimension of $1/T$ must be multiplied by k and $E_r e/m$ which has the dimensions of L/T^2 must be multiplied by k^2 in order to leave the solution for the path unchanged. In the same way, the conditions may be found for leaving the path unchanged when the electrode dimensions are altered. The results of this analysis may be summed up by the statement that the electron path will remain unchanged under any of the following conditions. (1) Changes of E and H which do not change E/H^2. (2) Changes of scale factor which include multiplication of E by the same factor. (3) Changes of scale factor which include division of H by the square root of the scale factor. It is to be understood in the above conditions that whenever the electrode potentials are changed the initial energy of the electron is to be changed by the same factor.

The procedure for setting up a model to represent quantitatively a given electron prob-

FIG. 4. Same as Fig. 3 with the addition of an initial velocity.

lem may now be briefly stated. First, let the model have the same linear dimensions as the original. Also, let H, E, A, C, $\dot{\Psi}$, and L be known quantities. There remains the adjustment of the values of F_r and F_ϕ so that the gyroscope will describe the same path as the electron. To do this, the difference in time scale between the model and the original is determined by the relation (see also (11a))

$$e/mH = kC/A\dot{\Psi}, \tag{12}$$

which defines k. From (12) and the first condition of invariance we can write (see also Eqs. (11a) and (11c))

$$e/mE_r = k^2L^2/AF_r, \tag{13a}$$

$$e/mE_\phi = k^2L^2/AF_\phi. \tag{13b}$$

These equations define F_r and F_ϕ and permit setting up a quantitative model having the same dimensions as the original. If the model is to be enlarged by a scale factor S over the original, then, according to the second invariance condition, the forces F_r and F_ϕ are to be multiplied by S. To summarize:

A model S times as large as the original may be set up so that the gyroscope describes corre-

spondingly the same path as the electron if

$$F_r = \frac{S}{k^2}\frac{L^2 e}{A m} E_r,$$

and

$$F_\phi = \frac{S}{k^2}\frac{L^2 e}{A m} E_\phi,$$

where

$$k = \frac{Ae}{Cm}\frac{H}{\dot{\Psi}}.$$

Application of the Model

The first part of this paper has described a model for tracing electron paths, defined the limits within which the model may be used, and obtained the quantitative relations between the model and the original. This much would be of academic interest only, unless some convenient means of setting up a force field to act on the gyroscope were available. The force field must, of course, approximate the electrostatic field in the original. Fortunately, such a field can easily be set up for many types of electrostatic fields by means of electromagnets with specially shaped pole faces. For example, to represent the electro-

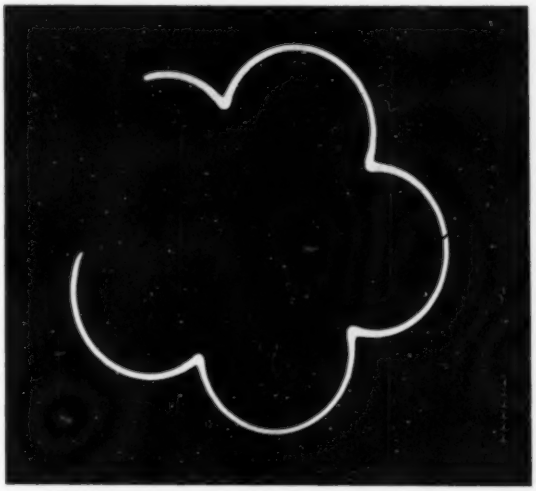

Fig. 5. Path of an electron in a central force field.

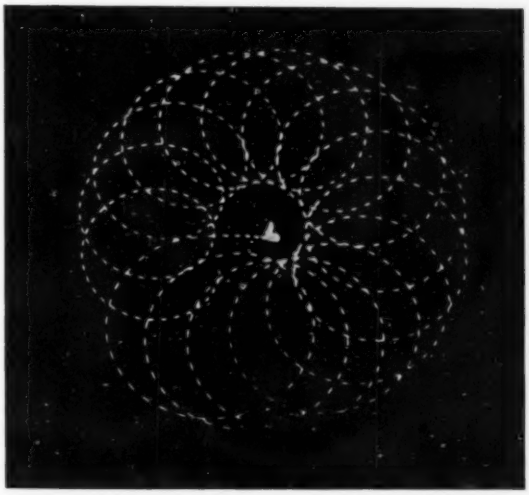

Fig. 6. Same as Fig. 5 with large initial velocity.

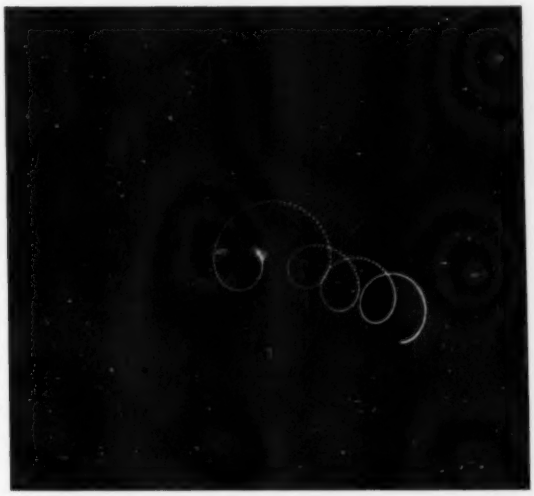

Fig. 7. Path of an electron in a magnetron. The lower plate is the less positive plate.

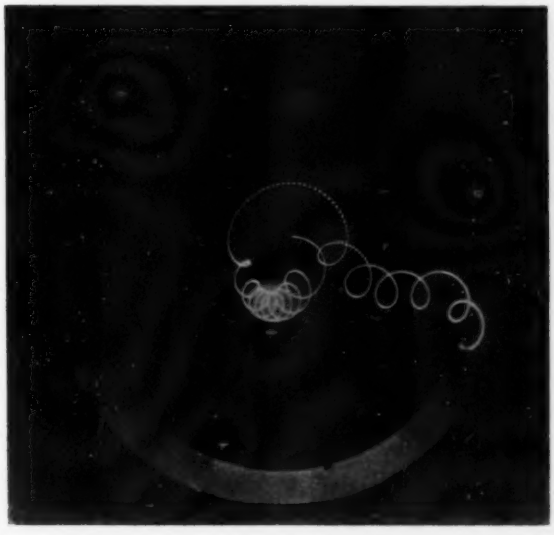

Fig. 8. Path of an electron in a magnetron showing electron "trapped" for an appreciable time in a low electric field region between cathode and the lower potential plate.

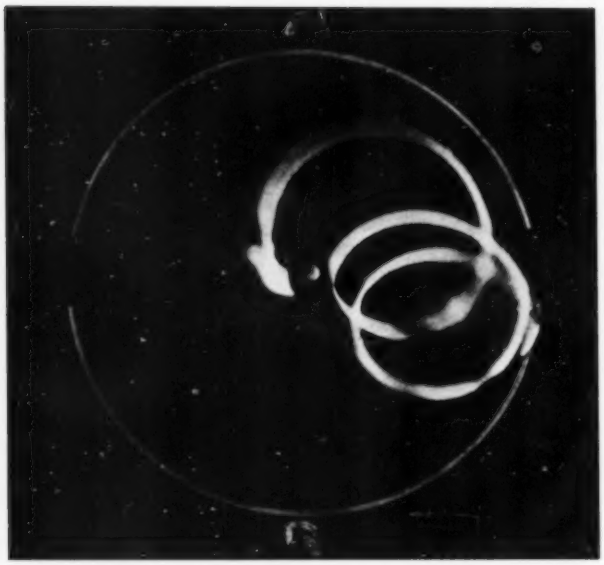

FIG. 9. Path of an electron beam in a magnetron as obtained by G. R. Kilgore using gas to make the beam visible.

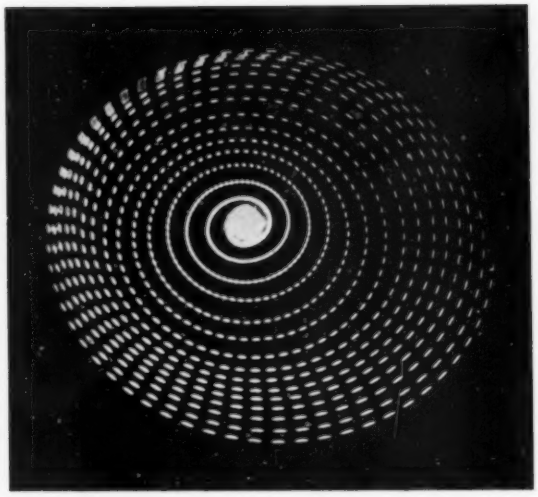

FIG. 10. Path of an electron in crossed electric and magnetic fields when the electric field is alternating in resonance with the angular period of the electron.

static field in a diode, an electromagnet with one pole connected to a soft-iron cylinder and the other to a soft-iron rod along the axis of the cylinder has been used. The electron has been represented by one pole of a long thin permanent magnet mounted so that one end is at the end of the gyroscope axis and the other end near the center of the gyroscope. This end contributes comparatively little to the moments of force acting on the axis both because it has a short lever arm and because it is somewhat removed from the external magnetic fields.

Another problem of practical importance is to mount the gyroscope so that there is a minimum of friction in the bearings. Friction in the spin axis bearings causes a slowing down of the spin velocity or in terms of the original, a continuously decreasing magnetic field. Friction in the gimbal bearings tends to damp out any rapid oscillations of the gyroscope and, in larger amounts, tends to introduce objectionable extraneous forces which permit the gyroscope axis to drift in the direction of the applied forces.

The gyroscope used to obtain the following paths is the small model made by the Sperry Gyroscope Company. The spin axis bearings were found to have sufficiently little friction so that even for small spin velocities the "magnetic field" remained substantially constant throughout a run. It was found necessary, however, to provide ball-bearing mountings for the gimbals to reduce their friction to a usable amount. The gyroscope and associated field apparatus to represent a magnetron are shown in Fig. 2. The end of the axis toward the "magnetron" has mounted on it a long thin Alnico magnet, the outer end of which represents the electron. A small flashlight bulb and battery are mounted on the other end of the axis for the purpose of photographing the path. A light chopper in front of the camera provides the time axis in the recorded picture of the path.

Figure 3 shows the familiar cycloidal motion of an electron in crossed electric and magnetic fields.[4] In Fig. 4, the same type of motion is recorded except that the "electron" was given an initial velocity. In all of these photographs the uniform magnetic field is normal to the plane of the picture.

The path of an electron, started from rest, in the radial electric field of a diode is shown in Fig. 5. In Fig. 6, the electric field is radial but generated by a point charge rather than a line charge. The electron was started very near the point charge and given an appreciable initial

[4] This type of motion is to be found in the electron multiplier described by V. K. Zworykin, G. A. Morton, and L. Malter, Proc. I. R. E. **24**, 361–370 (1936), and in the mass spectrograph described by W. Bleakney and J. A. Hipple, Jr., Phys. Rev. **53**, 521–529 (1938).

velocity. The gradual reduction in amplitude of successive loops is due to the small residual friction in the gimbal bearings. Two typical electron paths, under static conditions in a magnetron are shown in Figs. 7 and 8. The arrangement which generated the magnetron field can be seen in Fig. 2. The two plate sections were connected to opposite poles of an electromagnet, the upper plate being the more positive. A separate electromagnet in the form of a soft-iron rod served as the cathode. In both figures, it is to be noted that the electron lands on the lower potential plate. Figure 8, in particular, shows the electron trapped for an appreciable time in a region of low electric field between the cathode and lower potential plate. For comparison, an actual electron path in a magnetron as traced by an electron beam in gas is given in Fig. 9.[5] Figure 10 is of particular interest in showing the ability of the model to reproduce electron paths in alternating electric fields. A uniform magnetic field supplied by an electromagnet was periodically reversed by means of a motor-driven commutator in resonance with the motion of the gyroscope. Starting from rest, then, the electron described successively large circles as it gained energy from the alternating field. The fact that the light streaks are approximately lined up radially indicates that the angular velocity remained constant as the linear velocity was increased. (The angular velocity of an electron describing circles in a magnetic field is determined only by the magnetic field strength.) The slight ellipticity of the paths is the result of not having the moments of inertia of the gyroscope about the two sets of gimbal bearings exactly the same. The slight drift of the center of revolution towards one side is the result of a small d.c. electric field superposed on the alternating electric field.

These few illustrations show that the gyroscope may readily be used to give a semiquantitative demonstration of various types of electron paths in a uniform magnetic field and that for each type the initial velocities and field strengths may be conveniently varied to explore a wide range of conditions including zero magnetic field and alternating electric fields.

[5] This figure is reprinted by courtesy of the Institute of Radio Engineers from the paper, "Magnetron oscillators for the generation of frequencies between 300 and 600 megacycles," by G. R. Kilgore, Proc. I. R. E. **24**, 1145 (1936).

Notes on the Power Factor Testing of Long Lengths of Cables

ERIC A. WALKER
Department of Electrical Engineering, Tufts College Engineering School, Tufts College, Massachusetts
(Received February 16, 1940)

The ratio of watts to volt-amperes does not give the power factor of long cables because of the resistance of the conductor and sheath. The error involved varies as the length squared and might be quite appreciable at lengths of 10,000 feet. Correction factors are given involving the use of an infinite series for exact results and a simple algebraic formula for approximate results.

INTRODUCTION

A NUMBER of tests have been devised for determining the condition of insulation. The best known of these tests are the following: first, a direct-current resistance test made by means of a megger at several hundred volts;[1] second, a power-factor test made by means of a bridge or a watt-meter set; lastly, an overvoltage test. In this test a voltage several times the rated voltage of the equipment is applied to the insulation for a predetermined period of time. During this test the resistance may also be measured.

[1] *Megger Insulation-testing Instruments* (J. G. Biddle Company, Philadelphia, Pa., 1928).

THE ADVANTAGES AND DISADVANTAGES OF THE POWER FACTOR TEST

There are a number of reasons why the power-factor test is preferred. First of all, this

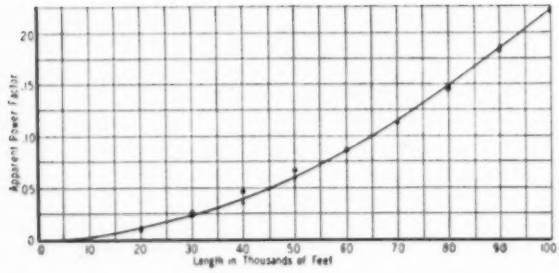

FIG. 1. Apparent power factor of a theoretical no-loss 1,000,000-cm 5-kv cable at 60 c.p.s.

type of test is made to determine the breakdown strength of the insulation and to ascertain its probable useful life. There appears to be little or no correlation between either of these properties and the direct-current resistance. However, both the life and the breakdown strength have been correlated with the power-factor of some materials.[2–4] Also power-factor is known to show certain types of faults which direct-current resistance tests will not reveal. The power-factor is independent of the amount of material being tested. As the power-factor test can be conducted at any voltage which the capacity of the testing equipment will allow, a voltage which will not injure nor destroy the insulation can be chosen. Lastly, the power-factor test has been used successfully on bushings and transformers in the field,[5] and on short lengths of cable in the laboratory.[6,7] A logical extension of the method is to apply the test to longer lengths of installed cable and to cables which have been in service in order to determine their present condition and life expectancy.

The limitations of the power-factor test are obvious. It is a test which gives a measure of the average condition of the cable. In other words, the test will not reveal a small section of deteriorated cable if it is tested as a part of a longer cable which is almost wholly in a satisfactory condition. In this respect the test is inferior to the overvoltage test which gives the breakdown strength of the weakest point if failure does take place. The second limitation is in the combination of high kva capacity which must be provided and the small amount of actual power which must be measured. For instance, a 5-kv varnished cambric cable with 1,000,000-cm conductor and insulation 0.109 inch thick will require about 4.25 kva charging capacity per 1000 feet of length if the test is made at 5 kv and 60 c.p.s. while the watts loss in the insulation at 0.02 power-factor will be of the order of 85 watts. However, apparatus does exist and tests have been made on lengths of cable up to five miles.

The third limitation, and the one with which this paper is concerned, is the effect of the resistance and inductance in the circuit being measured.

THE CIRCUIT CONSTANTS

In testing a cable by power-factor methods the path taken by the charging current must be studied in order to evaluate the circuit constants. Usually the charging current is fed from one end of the cable. This current flows out along the conductor, and returns through a path determined by several factors. If the cable is isolated and lies in a fiber duct the return path will be through the lead sheath. This makes the resistance of the return path quite appreciable. Of course, the resistance of the total return path may be much lower than the resistance of the lead sheath because of neighboring cables or other structures which provide an alternative ground return, or because of a copper binding

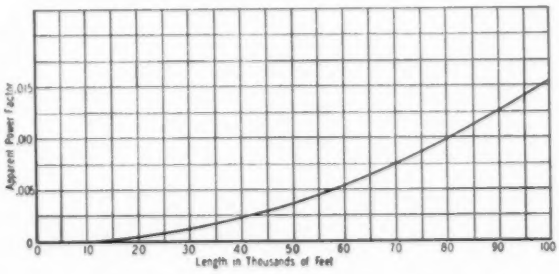

FIG. 2. Apparent power factor of a theoretical no-loss 0000 50-kv cable at 60 c.p.s.

[2] C. L. Dawes and F. L. Hoover, "Ionization studies in paper insulated cables. I," Trans. A.I.E.E. **45**, 141 (1926).
[3] C. L. Dawes, H. H. Reichard and P. H. Humphries, "Ionization studies in paper insulated cables. II," Trans. A.I.E.E. **48**, 382 (1929).
[4] B. L. Goodlet, F. S. Edwards and F. R. Perry, "Dielectric phenomena at high voltages," J. Inst. Elec. Eng. **69**, 695 (1931).
[5] I. W. Gross, "Field testing of bushing and transformer insulation by the power factor method," Trans. A.I.E.E. **57**, 589 (1938).
[6] G. B. Shanklin, "Compensated dynamometer wattmeter method of measuring dielectric energy loss," Gen. Elec. Rev. **19**, 842 (1916).
[7] E. S. Lee, "The use of a dynamometer wattmeter," Trans. A.I.E.E. **45**, 746 (1926).

tape around the insulation of the cable. One can only say then that the total resistance cannot be lower than the resistance of the center conductor or higher than the resistance of the conductor and the lead sheath. This resistance can be given in ohms per unit length or in ohms for the entire structure. For instance, the resistance per 1000 feet of conductor of the above cable is about 0.387 ohm.

The inductance of the circuit, if the current returns through the sheath, can be computed as the inductance of a concentric cable. An approximate formula, which neglects the thickness of the sheath is:

$$L=0.0305\left[0.5+2\ln\frac{R_2}{R_1}\right] \text{ millihenries per 1000 feet.}$$

If the return is not through the lead sheath but through other cables, or through ground, the inductance will be higher. The above formula gives the lower limit only. It is fortunate that later developments will show that this factor is not important.

The conductance and the susceptance of the insulation of the cable are the characteristics of the cable it is desired to measure. For small defect angles the power-factor is given by the ratio of these quantities:

$$\text{Power-factor}=\frac{\text{Conductance}}{\text{Susceptance}}=\frac{G}{B}. \qquad (1)$$

The question is, "Does a measurement at the end of a cable give this ratio?" In an attempt to answer this question the cable will be considered as an evenly distributed impedance, commonly called a smooth line.

The Development of an Exact and an Approximate Formula

Any measurement at the end of a cable will measure the input impedance of the cable, whether it is determined by a bridge or by a measurement of volts, amperes, and watts. The input impedance of a smooth line with the far end open is

$$Z_{\text{input}}=\frac{Z_0}{\tanh\theta}, \qquad (2)$$

or

$$Y_{\text{input}}=Y_0\tanh\theta, \qquad (3)$$

where

$$Z_0=(Z/Y)^{\frac{1}{2}};\quad Y_0=(Y/Z)^{\frac{1}{2}};\quad \theta=(ZY)^{\frac{1}{2}},$$

where $Z=R+jL\omega=R+jX$, the total series impedance of the cable, and $Y=G+jC\omega=G+jB$, the total parallel admittance of the cable.

Equation (3) can be expressed in a more convenient form:

$$Y_{\text{input}}=Y_0\tanh\theta=Y\frac{\tanh\theta}{\theta}. \qquad (4)$$

This is an exact equation for any smooth line. The equation can be expanded in an infinite series:

$$\begin{aligned}Y_{\text{input}}&=Y\left[1-\frac{ZY}{3}+\frac{2}{15}Z^2Y^2\cdots\right]\\&=(G+jB)\left[1-\frac{(RG-BX)+j(RB+GX)}{3}\text{etc.}\right].\end{aligned} \qquad (5)$$

A test with actual numerical values shows that for a wide range of values this equation reduces to the following approximate formula:

$$Y_{\text{input}}=G+\frac{RB^2}{3}+jB. \qquad (6)$$

Then Eq. (1) becomes:

$$\text{Observed power-factor}=\frac{G}{B}+\frac{RB}{3}. \qquad (7)$$

Let the observed power factor $=\delta'$ and the real power factor $G/B=\delta$. Then

$$\delta=\delta'-\frac{RB}{3}. \qquad (8)$$

This equation shows that the observed power-factor is too high by a correction factor depending on the resistance and susceptance of the cable. It does not depend on the inductance. The correction factor also increases as the square of the length of the cable.

If the volts amperes and watts are read for the cable the equation becomes:

$$\delta=\frac{\text{watts}}{\text{volt-amperes}}\left[1-\frac{I^2R}{3}\right]. \qquad (9)$$

In Fig. 1 the apparent power-factor of the cable already described is shown for lengths up to

100,000 feet, on the assumption that the cable had zero power-factor. This figure then shows the amount which must be subtracted from the observed power-factor of a cable of these dimensions in order to determine the real power-factor. In this figure, the correction factor as determined by Eq. (8) is indicated by the crosses, while the circles give the exact correction factor found by using as many terms as are significant in Eq. (5). It is seen that the agreement is fairly good.

Figure 2 shows the same sort of curve for another type of cable. This cable has dimensions quite different from those of Fig. 1 and it was chosen to show that Eq. (8) is valid for widely different types of cables.

Conclusions

For long cables the power-factor as observed at one end must be corrected to give the true power-factor of the insulation.

Although the correction factor is not important for short lengths, it is important for lengths of cable of the order of 10,000 ft.

The resistance of the return path of the current has considerable influence on the correction factor.

The inductance of the cable has little effect on the measured values.

The correction factor will be higher at higher frequencies.

A simplified equation for computing this correction factor is quite satisfactory.

Similarity of the Stress Distributions in a Circular Disk and a Square Plate

H. Ôkubo
Technical College, Yonezawa, Japan
(Received April 18, 1940)

MANY a solution has been carried out for a circular disk compressed diametrically. But few solutions for a square plate were found formerly. In this paper we will introduce a solution which is more convenient for numerical calculations than the solutions of the previous authors, and show that the stress distribution in a square plate compressed by a pair of opposite forces acting on its two sides is similar to the one in a circular disk compressed diametrically.

The generalized plane stress in a plate is generally given by[1]

$$\left.\begin{aligned} X_x &= -\lim_{k\to 1} \Re[k^2\varphi_1(x+iky)+\varphi_2(x+iy)], \\ Y_y &= \lim_{k\to 1} \Re[\varphi_1(x+iky)+\varphi_2(x+iy)], \\ X_y &= \lim_{k\to 1} \Im[k\varphi_1(x+iky)+\varphi_2(x+iy)], \end{aligned}\right\} \tag{1}$$

where φ_1 and φ_2 are two arbitrary functions determined to satisfy the boundary conditions, $\Re$ and $\Im$ denote, respectively, the real part and the imaginary part divided by i of a function directly following them.

When a square plate of side length 2 is compressed by a pair of opposite forces P acting on its two sides at their centers as is shown in Fig. 1, the boundary conditions are

$$\left.\begin{aligned} X_x &= 0, & X_y &= 0, \quad \text{when } x=\pm 1, \\ Y_y &= -\frac{P}{2} - P\sum_{n=1}^{\infty} \cos n\pi x, & X_y &= 0, \quad \text{when } y=\pm 1. \end{aligned}\right\} \tag{2}$$

[1] H. Ôkubo: Science Reports of the Tôhoku Imperial University, Series 1, XXV. No. 5 (March 1937).

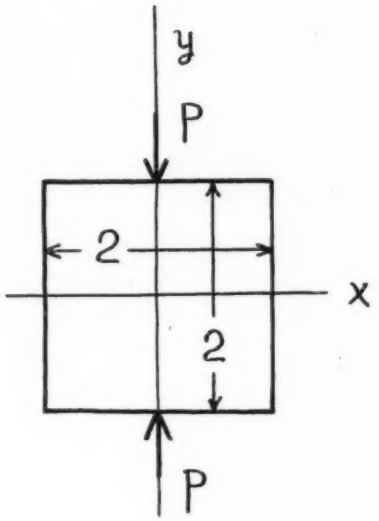

FIG. 1.

TABLE I.

$P_0 = -0.5$	
$P_1 = -1.047$	$Q_1 = 0.255$
$P_2 = -0.963$	$Q_2 = -0.116$
$P_3 = -1.026$	$Q_3 = 0.051$
$P_4 = -0.981$	$Q_4 = -0.029$
$P_5 = -1.014$	$Q_5 = 0.017$
$P_6 = -0.989$	$Q_6 = -0.010$
$P_7 = -1.009$	$Q_7 = 0.005$
$P_8 = -0.993$	$Q_8 = 0.000$
$P_9 = -1.006$	$Q_9 = -0.002$
$P_{10} = -0.996$	$Q_{10} = -0.001$
$P_{11} = -1.004$	$Q_{11} = -0.006$
$P_{12} = -0.997$	$Q_{12} = 0.007$

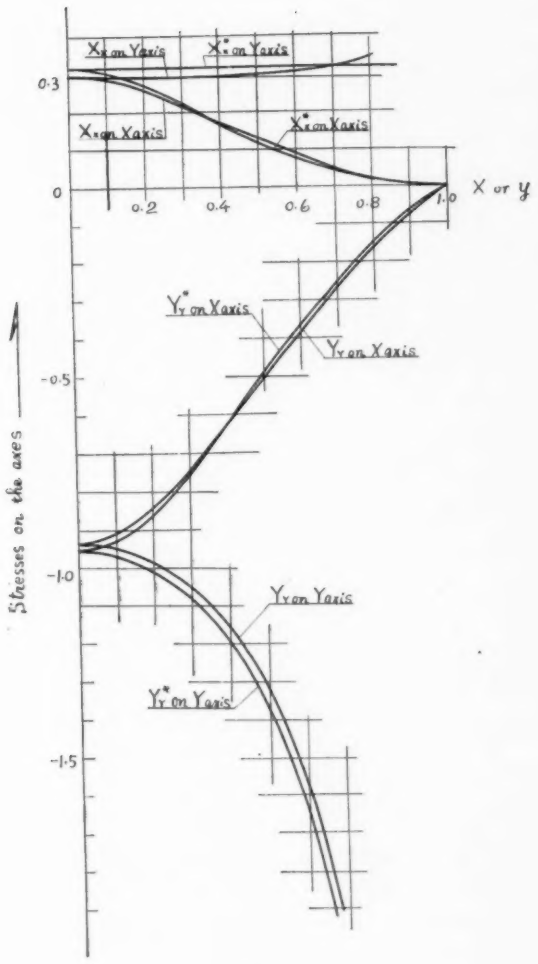

FIG. 2.

Now putting

$$\left.\begin{aligned}\varphi_1(x+iky) &= \sum_{n=0}^{\infty} A_n \cos n\pi(x+iky),\\ \varphi_2(x+iy) &= \sum_{n=0}^{\infty} B_n \cos n\pi(x+iy).\end{aligned}\right\} \tag{3}$$

The stresses (1) satisfy the boundary conditions

$$Y_y = \sum_{n=0}^{\infty} P_n \cos n\pi x, \quad X_y = 0, \quad \text{when } y = \pm 1, \tag{4}$$

if

$$\left.\begin{aligned}A_n &= \frac{P_n \sinh n\pi}{\cosh n\pi k \sinh n\pi - k \sinh n\pi k \cosh n\pi},\\ B_n &= \frac{-kP_n \sinh n\pi k}{\cosh n\pi k \sinh n\pi - k \sinh n\pi k \cosh n\pi}.\end{aligned}\right\} \tag{5}$$

TABLE II.

x	y	x_x	y_y	x_x^*	y_y^*
0	1.00		$-\infty$	0.318	$-\infty$
0	0.75	0.328	−2.551	0.318	−2.592
0	0.50	0.298	−1.322	0.318	−1.379
0	0.25	0.296	−1.017	0.318	−1.040
0	0	0.296	−0.939	0.318	−0.955
0.25	0	0.231	−0.800	0.248	−0.809
0.50	0	0.103	−0.503	0.115	−0.497
0.75	0	0.027	−0.214	0.025	−0.202
1.00	0	0	0	0	0

Inserting A_n, B_n given by (5) into (1), we have

$$\left.\begin{aligned} X_x &= \sum_{n=0}^{\infty} P_n \xi_n(y) \cos n\pi x, \\ Y_y &= \sum_{n=0}^{\infty} P_n \eta_n(y) \cos n\pi x, \\ X_y &= \sum_{n=0}^{\infty} P_n \zeta_n(y) \sin n\pi x, \end{aligned}\right\} \tag{6}$$

where

$$\xi_n(y) = \frac{\sinh n\pi \cosh n\pi y + n\pi y \sinh n\pi \sinh n\pi y - n\pi \cosh n\pi \cosh n\pi y}{\sinh n\pi \cosh n\pi + n\pi},$$

$$\eta_n(y) = \frac{\sinh n\pi \cosh n\pi y - n\pi y \sinh n\pi \sinh n\pi y + n\pi \cosh n\pi \cosh n\pi y}{\sinh n\pi \cosh n\pi + n\pi},$$

$$\zeta_n(y) = \frac{n\pi \cosh n\pi \sinh n\pi y - n\pi y \sinh n\pi \cosh n\pi y}{\sinh n\pi \cosh n\pi + n\pi}.$$

On the sides $x = \pm 1$, the shear vanishes and the normal tension is

$$X_x = \sum_{n=1}^{\infty} P_n (-1)^n \xi_n(y),$$

which is expanded in Fourier's cosine series and given by

$$X_x = -\sum_{j=1}^{\infty} Q_j \cos j\pi y, \tag{7}$$

where

$$Q_j = \sum_{n=1}^{\infty} P_n (-1)^{n+1} I(n, j), \quad I(n, j) = \frac{4(-1)^j n j^2 \sinh^2 n\pi}{\pi (n^2 + j^2)^2 (\sinh n\pi \cosh n\pi + n\pi)}. \tag{8}$$

Similarly we can find the stresses which satisfy the following boundary conditions

$$X_x = \sum_{j=1}^{\infty} Q_j \cos j\pi y, \quad X_y = 0, \quad \text{when } x = \pm 1,$$

as

$$\left.\begin{aligned} X_x &= \sum_{j=1}^{\infty} Q_j \eta_j(x) \cos j\pi y, \\ Y_y &= \sum_{j=1}^{\infty} Q_j \xi_j(x) \cos j\pi y, \\ X_y &= \sum_{j=1}^{\infty} Q_j \zeta_j(x) \sin j\pi y. \end{aligned}\right\} \tag{9}$$

On the sides $y=\pm 1$, the shear vanishes and the normal tension is

$$Y_y=\sum_{j=1}^{\infty} Q_j(-1)^j\xi_j(x)=\sum_{m=1}^{\infty} R_m \cos m\pi x,$$

where

$$R_m=\sum_{j=1}^{\infty} Q_j(-1)^j I(j, m).$$

The stress system (6) superposed with (9) satisfies the boundary condition (2), if

$$P_n+\sum_{m=1}^{\infty} P_m(-1)^{m+1}\sum_{j=1}^{\infty}(-1)^j I(j, n)I(m, j)+P=0. \tag{10}$$

From Eq. (10) we can determine P_n, and inserting them into (8) we can find Q_j, all the unknown constants are known. Values of P_n and Q_j calculated from Eqs. (8) and (10) are given in Table I.

The stress system (6) superposed with (9) is

$$\left.\begin{aligned} X_x&=\sum_{n=1}^{\infty}\{P_n\xi_n(y)\cos n\pi x+Q_n\eta_n(x)\cos n\pi y\},\\ Y_y&=-\frac{P}{2}+\sum_{n=1}^{\infty}\{P_n\eta_n(y)\cos n\pi x+Q_n\xi_n(x)\cos n\pi y\},\\ X_y&=\sum_{n=1}^{\infty}\{P_n\zeta_n(y)\sin n\pi x+Q_n\zeta_n(x)\sin n\pi y\}. \end{aligned}\right\} \tag{11}$$

Values of stresses on the x and y axes are calculated from the above equations and tabulated in Table II and are plotted in Fig. 2 (* shows the values in a circular disk). From the figure it is obvious that the stress distribution on the axes are closely similar with the one on the horizontal and vertical diameters of a circular disk of radius unity under the cognate boundary conditions. If that is compared with the fact that the stress distribution in an elliptic plate with an eccentricity near unity is not similar to the one in a circular disk,[2] the result is very interesting.

In conclusion, the writer wishes to express his thanks to Mr. S. Ôba, Head of the Yonezawa Technical College for his encouragement throughout the investigation.

[2] H. Ôkubo, Phil. Mag. **27**, 508 (1939).

Stress Analysis by Three-Dimensional Photoelastic Methods*

DANIEL C. DRUCKER AND RAYMOND D. MINDLIN
Department of Civil Engineering, Columbia University, New York, New York
(Received June 13, 1940)

This paper describes the results of an investigation and extension of the various proposed procedures and methods of analysis for the photoelastic determination of three-dimensional states of stress. Two important limitations of the previous developments are removed. A true extension to three dimensions is given by the determination of the effect on retardation of appreciable variation in the orientation of the secondary principal stresses in planes perpendicular to the wave normal (such variation being the rule rather than the exception for general states of stress). Also, methods for the analysis of whole planes are presented, thus avoiding the cumbersome and tedious point by point procedures that have been advanced. In the particular case of plane stress, these methods reduce to a purely optical technique for determining the principal stresses themselves, or more easily their sum, for the entire model.

INTRODUCTION

TWO general practical methods have been proposed, and to some extent used, for the photoelastic determination of three-dimensional states of stress. In one, the stresses are "frozen" in the model and slices cut from it are analyzed; in the other, the phenomenon of scattering of light is employed. The technique of measurement required is different for the two cases and therefore they will be discussed separately. However, both methods depend upon the effects of stress on the propagation of light, and these are the same regardless of the method of observation. In the previous developments of the theory, only those effects were considered which are present in ordinary two-dimensional states of stress.

These effects in three-dimensional states of stress differ considerably from those present in the usual two-dimensional case. The rotation along the wave normal of the axes of secondary principal stress[1] in planes perpendicular to the wave normal is the principal cause of the difference and has not been considered previously.

Knowledge of what occurs in general states of stress permits broadening of the methods of observation to include entire planes rather than confining attention to a single point at a time.

WELLER'S METHOD

If one wishes to analyze a three-dimensional state of stress in a model under actual load, the only practical method of general application available at present is that proposed by Weller.[2] This method is based upon the fact that in a transparent medium, light scattered at right angles to the incident wave normal is plane polarized, the amplitude of the vibration reaching the eye of an observer being proportional to the projection of the light vector on the plane perpendicular to the direction of observation. The result is similar to that produced by the analyzer in a polariscope. (See Fig. 1.) If the light incident at a point is plane polarized, the intensity of scattered light observed at right angles to the wave normal will thus vary from zero when looking along the direction of vibration to a maximum when looking perpendicularly to this direction.

When photoelastic materials are stressed they become doubly refracting and, for a given wave normal, light can be transmitted only in vibrations along two mutually perpendicular axes lying in the planes perpendicular to the wave normal. These directions, which we may designate as the axes of secondary principal stress[1] are determined in the same manner as the principal directions for plane stress. (The normal and shearing stresses acting on the planes perpendicular to the wave normal need not be considered in measuring or calculating secondary principal stresses as the former may be varied

* Publication assisted by the Ernest Kempton Adams Fund for Physical Research of Columbia University.

[1] R. D. Mindlin, "A review of the photoelastic method of stress analysis," J. App. Phys. **10**, 229 (1939).

[2] R. Weller, "A new method for photoelasticity in three dimensions," J. App. Phys. **10**, 266 (1939). "Three-dimensional photoelastic analysis by scattered light," Papers presented at the 9th meeting of the Eastern Photoelasticity Conference, May 1939, p. 19.

at will without changing the latter, even though such variation changes the magnitudes and directions of the true principal stresses.) The light scattered from any point (O, Fig. 1) can therefore be considered as coming from two plane polarized vibrations (along p and q) differing in phase by an amount depending upon the integrated optical properties of the material along the path from the point of entrance (O') into the model to the point at which the scattering occurs. In general the two vibrations combine to form an elliptical vibration, the plane of the ellipse being perpendicular to the wave normal. The intensity of the light scattered at right angles to the wave normal is proportional to the square of the length of the projection (e.g., QQ or TT) of this ellipse on a plane perpendicular to the direction of observation.

If a whole plane of the model is illuminated by a sheet of parallel rays of polarized light formed by passage through a polarizer, collimator, and a slit, the light scattered in a given direction perpendicular to the wave normal will in general vary in intensity from point to point in the plane depending upon the projections of the ellipse of vibration associated with each point in the plane, the alternate lighter and darker regions forming a fringe pattern. This interference pattern will vary in distinctness and even in form as the direction of observation is changed, but in general it may be said that the distance between fringes in the direction of travel of the light is a function of the state of stress between the points of minimum intensity.

Weller's method for a general state of stress is to fix attention on any point desired and rotate the model until the minimum distance between fringes straddling the point is obtained. If the stress field is perfectly uniform in the vicinity, this minimum distance gives the maximum principal stress difference at the point according to the simple relation[3]

$$\sigma_3-\sigma_1=\frac{C}{d}, \qquad (1)$$

where σ_3 and σ_1 are the algebraically largest and least principal stresses, respectively, C is the stress optical coefficient in stress units per unit thickness per fringe, and d is the distance between fringes measured along the wave normal, i.e., along the direction of the intermediate principal stress σ_2. The formula and reasoning are exactly the same as in two-dimensional work.

If σ_3 and σ_1 vary in magnitude along the wave normal, but remain fixed in direction, the stress

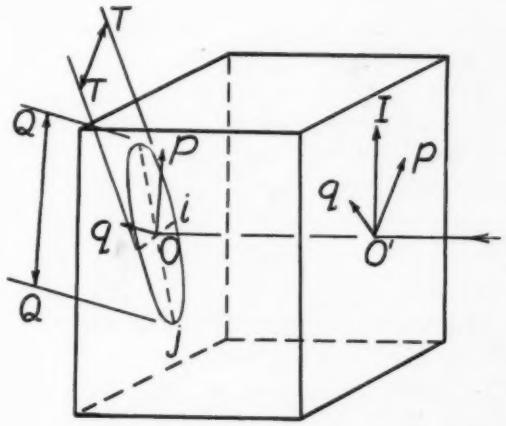

FIG. 1. Scattering of light. The entering vibration OI' breaks up into two components, one along p, the other along q. At any point O in the model the two components in general will combine to form an elliptic vibration with axes Oi and Oj in the plane perpendicular to the wave normal $O'O$. The intensity of scattered light seen by an observer is proportional to the square of the projection of the ellipse (e.g., QQ or TT) on a plane perpendicular to the direction of observation.

found from Eq. (1) will exist at some point intermediate between the two fringes. For small gradients of stress magnitude, the midpoint is close enough. If greater accuracy should be desired, plotting the fringe positions against their order will determine the point more closely.

If the orientations of the principal stresses do not vary, there is no theoretical objection to Weller's proposal. However, as will be shown in the following section, if there is rotation along the wave normal of the axes of primary or secondary principal stress in planes perpendicular to the wave normal, the distance between fringes is no longer dependent solely on the magnitudes of the stresses and Eq. (1) or its equivalent for secondary principal stress is no longer valid.

[3] R. Weller and J. K. Bussey, "Photoelastic analysis of three-dimensional stress systems using scattered light," Tech. Note No. 737 N. A. C. A.

As we are interested in determining the effect of rotation of the axes of primary or secondary principal stress, it is desirable to strip the problem of all stress variables except orientation. The fundamental case to be considered is thus one in which the magnitudes of the stresses remain fixed while their orientations, in planes perpendicular to the wave normal, change at a constant rate along the wave normal. In any case we have to solve a problem of wave propagation in a nonhomogeneous, nonisotropic medium. The mathematical formulation of such problems generally leads to a system of simultaneous, linear, partial differential equations of the second order with variable coefficients.

The differential equations may be formulated in terms of an elastic ether theory of light. From a general point of view, this theory is not the most satisfactory one available; but it is very convenient for photoelasticity as it is based upon the ideas of stress, strain, and displacement, and upon the equations of motion with which workers in elasticity and photoelasticity are familiar. The resulting differential equations are exactly the same as those obtained from the electromagnetic theory of light if the symbols representing displacement, density, and shear modulus are interpreted as magnetic force, magnetic permeability, and reciprocal of dielectric coefficient, respectively.

The equations of motion in terms of the stresses are

$$\left.\begin{aligned}
\frac{\partial \sigma_x'}{\partial x}+\frac{\partial \tau_{xy}'}{\partial y}+\frac{\partial \tau_{xz}'}{\partial z}&=\rho\frac{\partial^2 u'}{\partial t^2}\\
\frac{\partial \tau_{xy}'}{\partial x}+\frac{\partial \sigma_y'}{\partial y}+\frac{\partial \tau_{yz}'}{\partial z}&=\rho\frac{\partial^2 v'}{\partial t^2}\\
\frac{\partial \tau_{xz}'}{\partial x}+\frac{\partial \tau_{yz}'}{\partial y}+\frac{\partial \sigma_z'}{\partial z}&=\rho\frac{\partial^2 w'}{\partial t^2}
\end{aligned}\right\}, \qquad (2)$$

where σ_x', σ_y', σ_z', τ_{xy}', τ_{yz}', τ_{zz}' are the ether stresses, u', v', w' are the ether displacements, and ρ is the density.

The ether stresses may be expressed in terms of the ether displacements and the elastic coefficients of the ether by three equations of the type[4]

$$\sigma_x'=-2G_3\frac{\partial v'}{\partial y}-2G_2\frac{\partial w'}{\partial z}+2E_1\left(\frac{\partial v'}{\partial z}+\frac{\partial w'}{\partial y}\right) \qquad (3)$$

and three of the type

$$\tau_{yz}'=2E_1\frac{\partial u'}{\partial x}+G_1\left(\frac{\partial v'}{\partial z}+\frac{\partial w'}{\partial y}\right)-E_3\left(\frac{\partial w'}{\partial x}+\frac{\partial u'}{\partial z}\right)-E_2\left(\frac{\partial u'}{\partial y}+\frac{\partial v'}{\partial x}\right). \qquad (4)$$

The elastic coefficients (the E_i and G_i) are variables for a nonhomogeneous medium. They are related to the principal wave velocities a, b, c by equations of the type

$$a^2=\frac{G_1'}{\rho}, \qquad (5)$$

in which G_1' is a stationary value of the G_i.

Finally, the principal velocities a, b, c are determined from the stress-optical laws[5] by three equations of the type

$$a^2=v_0^2+\alpha(\sigma_2+\sigma_3)+\beta\sigma_1, \qquad (6)$$

in which v_0 is the velocity in the unstressed medium and α and β are stress-optical coefficients, constant for a given material and wavelength, λ, of light.

Considering a Cartesian coordinate system x, y, z with the origin at entrance to the medium, the simplest state of stress that will satisfy the conditions of the present problem is a simple tension, $\sigma=\sigma_3$, in the yz-plane inclined to the z axis at a variable angle $\varphi=(A/2)x$, where A is a constant. If the wave normal is in the direction of the x axis, $\Delta=(2\pi\sigma/C)x=2kx$ is the relative retardation in radians caused by the magnitude of σ alone. The ratio of rotation to retardation is φ/Δ a constant which we shall call $R/2$.

Using these specifications for the state of stress, and combining Eqs. (2), (3), (4), (5), and (6) we find the following simultaneous differential equations for v' and w':

[4] M. G. Lamé, *Leçons sur la Théorie Mathématique de l'Élasticité* (Paris, 1866), p. 231.

[5] E. G. Coker and L. N. G. Filon, *Treatise on Photoelasticity* (Cambridge University Press, 1931), p. 198.

$$\left.\begin{aligned}\frac{\partial^2 v'}{\partial t^2}&=H\frac{\partial^2 v'}{\partial x^2}-B\cos Ax\frac{\partial^2 v'}{\partial x^2}+BA\sin Ax\frac{\partial v'}{\partial x}\\&\quad+B\sin Ax\frac{\partial^2 w'}{\partial x^2}+BA\cos Ax\frac{\partial w'}{\partial x}\\\frac{\partial^2 w'}{\partial t^2}&=H\frac{\partial^2 w'}{\partial x^2}+B\cos Ax\frac{\partial^2 w'}{\partial x^2}-BA\sin Ax\frac{\partial w'}{\partial x}\\&\quad+B\sin Ax\frac{\partial^2 v'}{\partial x^2}+BA\cos Ax\frac{\partial v'}{\partial x}\end{aligned}\right\}\quad(7)$$

in which

$$B=\left(\frac{\alpha-\beta}{2}\right)\sigma,\quad H=v_0^2+\left(\frac{\alpha+\beta}{2}\right)\sigma.$$

Equations (7) may be reduced to equations with constant coefficients by referring the dependent variables to the axes of principal stress. Calling the displacements along the 2 and 3 axes (perpendicular and parallel to the direction of σ) v and w, we find

$$\left.\begin{aligned}F\frac{\partial^2 v}{\partial x^2}-\frac{A^2D}{4}v+HA\frac{\partial w}{\partial x}&=\frac{\partial^2 v}{\partial t^2}\\D\frac{\partial^2 w}{\partial x^2}-\frac{A^2F}{4}w-HA\frac{\partial v}{\partial x}&=\frac{\partial^2 w}{\partial t^2}\end{aligned}\right\}\quad(8)$$

in which

$$F=v_0^2+\beta\sigma=H-B;\quad D=v_0^2+\alpha\sigma=H+B.$$

The independent variables may be separated in the usual manner by setting

$$\left.\begin{aligned}v&=V(x)e^{\pm i\omega t}\\w&=W(x)e^{\pm i\omega t}\end{aligned}\right\}\quad(9)$$

and, finally, the dependent variables V and W may be separated by differentiation and addition of the two resulting equations. This results in the same fourth-order linear differential equation with constant coefficients for both V and W:

$$DF\frac{\partial^4 V}{\partial x^4}+\left[(D+F)\omega^2-\frac{A^2}{4}(D^2+F^2)+H^2A^2\right]\frac{\partial^2 V}{\partial x^2}+\left[\omega^4-\frac{A^2\omega^2}{4}(D+F)+\frac{A^4}{16}DF\right]=0.\quad(10)$$

The exact solution of this equation is so cumbersome that it is quite unusable. It can however be simplified by taking into account the orders of magnitude of the quantities involved. If the product $2k\lambda$ is much less than unity, most of the terms in the solution disappear. Even in highly stressed Bakelite, $2k\lambda$ will be less than 0.01 so that the simplification is justified, especially so as the square of the term appears and not the term itself.

Considering only the forward traveling waves and taking $v=M\cos\omega t$ at $x=0$, we then find

$$v=[K\sin kSx+M\cos kSx]\cos\left(\omega t-\frac{\omega}{\sqrt{H}}x\right)+(L\sin kSx)\sin\left(\omega t-\frac{\omega}{\sqrt{H}}x\right),\quad(11)$$

where $S=(1+R^2)^{\frac{1}{2}}$ and K and L are constants. Taking $w=N\cos\omega t$ at $x=0$, the same equation will hold for w except for constants. Thus there are four constants to be determined. They can be obtained in terms of M and N by substituting in Eqs. (8). When this is done, apparently eight relations exist among the four constants. Making the assumption above as to the magnitude of the retardation and also a similar one for the magnitude of $A=2\varphi/x$ and also for $S=(1+R^2)^{\frac{1}{2}}$, the eight relations reduce to four which determine the constants uniquely. Even if a rotation of axes of 360° takes place within a distance as small as a millimeter, and if $2k$ is as small as one-tenth of a fringe per inch, λA and λS are small compared to unity and can be neglected, so that the assumptions are entirely justified.

v and w can then be expressed in terms of their initial amplitudes M and N as follows:

$$\left.\begin{aligned}v&=\left[-\frac{R}{S}N\sin kSx+M\cos kSx\right]\times\cos\left(\omega t-\frac{\omega}{\sqrt{H}}x\right)-\left(\frac{M}{S}\sin kSx\right)\sin\left(\omega t-\frac{\omega}{\sqrt{H}}x\right)\\w&=\left[+\frac{R}{S}M\sin kSx+N\cos kSx\right]\times\cos\left(\omega t-\frac{\omega}{\sqrt{H}}x\right)+\left(\frac{N}{S}\sin kSx\right)\sin\left(\omega t-\frac{\omega}{\sqrt{H}}x\right)\end{aligned}\right\}\quad(12)$$

assuming them to be in phase on entrance. If φ is set equal to zero these reduce to the expressions which would be obtained for simple tension along z. If v and w have an arbitrary phase relation on entrance, it is only necessary to add a phase constant ϵ to the terms multiplied by M and another phase constant ϵ' to the terms multiplied by N. For example, if circularly polarized light enters the model, $\pi/2$ is added to the phase of either the M or N terms depending upon whether the polarization is right or left, and M is then set equal to N. The term $(\omega/\sqrt{H})x$ appears in all of the phase angles with the same sign and therefore has no influence on the relative retardation.

From Eqs. (12) for the components of vibration, or more clearly from the combined form

$$\left.\begin{aligned} v=&-\frac{R}{S}N\sin kSx\cos\left(\omega t-\frac{\omega}{\sqrt{H}}x\right)\\ &+\left[M\left(1-\frac{R^2}{S^2}\sin^2 kSx\right)^{\frac{1}{2}}\right]\\ &\times\cos\left[\omega t-\frac{\omega}{\sqrt{H}}x+\arctan\left(\frac{\tan kSx}{S}\right)\right]\\ w=&+\frac{R}{S}M\sin kSx\cos\left(\omega t-\frac{\omega}{\sqrt{H}}x\right)\\ &+\left[N\left(1-\frac{R^2}{S^2}\sin^2 kSx\right)^{\frac{1}{2}}\right]\\ &\times\cos\left[\omega t-\frac{\omega}{\sqrt{H}}x-\arctan\left(\frac{\tan kSx}{S}\right)\right] \end{aligned}\right\}\quad(13)$$

it may be seen that, wherever $\tan kSx=0$, v and w are in phase. This requires $kSx=n\pi$, or $x=n\pi/kS$. The distance between points in phase is thus $d=\pi/kS$. Now π/k is the spacing one would find if only the magnitude of the stresses affected the retardation, so that the factor $1/S$ is the effect of rotation. Hence the distance between points of equal phase is decreased, or conversely the retardation is increased by rotation. Intensity expressions for either plane or circularly polarized light on entrance can be set up. From these it is found that minima of intensity occur at intervals of π/kS for observation in any direction fixed in space or for a direction rotating with the axes of principal stress.

The same results were obtained by a quite different method of approach which is of value because of its closer physical connection with the problem. A series of parallel identical crystal plates (corresponding to constant magnitude of principal stresses) each with its polarizing axes inclined at a constant angle to those of the previous plate (uniform rotation of the axes of principal stress) was considered. If the number of plates is made infinite while the total relative retardation due to the magnitude of the stresses and the total rotation remain finite, the conditions of the problem are satisfied.

There are two essential parts to the solution. First, general expressions are obtained for the vibrations along each of the two crystal axes in any plate by a deductive-inductive process; second, the limits of these expressions, in usable form, are found as the number of plates becomes infinite. Both of these steps are rather long and involved. A doubly infinite series must be set up and then summed. Series of Bessel functions of the zero and first order appear, which reduce eventually to the simple trigonometric terms of Eq. (12).

It is of interest to note that the justifiable assumptions as to the magnitudes of the rotation and retardation found necessary in the previous method do not appear explicitly in this one though obviously they must be contained in it.

From Eq. (12) we see that if the entering vibration coincides with an initial direction of principal stress, say the p direction, then the vibration along q at any point is given by

$$w=\left(\frac{R}{S}M\sin kSx\right)\cos\left(\omega t-\frac{\omega}{\sqrt{H}}x\right).\quad(14)$$

If the ratio, $R/2$, of the rotation to the retardation (due to the magnitude of stress) is small, even though the magnitude of the rotation itself be large, the intensity along q will be very small, the light will be approximately plane polarized at all points. The light vector may be said to follow along the direction of principal stress, i.e., practically no light will be scattered in this direction. The eye of an observer moving along a helix (the intersection of a line along the

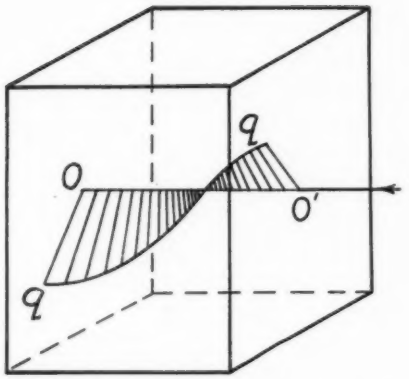

FIG. 2. The light vector follows the axis of principal stress. $O'q$—entering direction of vibration of light coincides with a principal axis of stress.

principal axis of stress with a cylinder having the points observed as its axis) will perceive a continuous dark band. (See Fig. 2.)

Equation (14) shows that even if the ratio of rotation to retardation is high, the intensity along q is zero wherever the vibration is plane polarized. There is a following around of the light vector, but between the points of plane polarization the intensity along q may be high. Fringes will therefore appear when there is rotation even though the entering vibration coincides with an initial direction of principal stress, while if there is no rotation, uniform intensity will prevail no matter what the direction of observation. Furthermore, the spacing of the fringes will be the same as the spacing when the entering light has components along both p and q.

The distance between fringes is decreased due to the rotation of the axes of principal stress. As can be seen from Eqs. (12) and (13), plane polarization or circular polarization will reoccur at intervals given by:

$$d=\frac{\pi}{k}\cdot\frac{1}{S}. \tag{15}$$

The retardation is thus seen to be increased by the factor $S=(1+R^2)^{\frac{1}{2}}$ where $R=2\varphi/\Delta$, or the distance between fringes decreased by $1/S$. The difference between the secondary principal stresses in the general case is thus

$$\sigma_p-\sigma_q=\frac{C}{d}\cdot\frac{1}{S}, \tag{16}$$

which is to be compared with Eq. (1). As S can be quite large, neglect of it may, in many cases, produce appreciable error, though on the "safe" side as the apparent stress will be higher than the true. If the total rotation is small, the formulas show that in practical cases it may be neglected as far as its effect on the distance between fringes is concerned. Usually one is interested in regions of high stress where the fringes will be closely spaced. In such cases, the total rotation probably will not be very large and the ratio of rotation to retardation probably small, though often appreciable in effect.

While true extinction will occur only if the eye follows the directions of principal stress in a helix, it is nevertheless true that for a fixed direction of observation, minima will occur at the same spacing as given in (15) and although the fringe pattern will not be as distinct it will yield the same results. The amount of rotation between two fringes may be obtained by finding the difference in the orientations for which each appears darkest.

Analysis of General States of Stress

Having the interpretation of fringe spacing in terms of stress magnitude and rotation of axes, it is possible to consider the procedures proposed for making the necessary optical measurements. Weller's suggestion of universal rotation of the model while under load would require a very complicated loading device. Also, the stress at only one point at a time would be determined. The suggestion is therefore advanced that whole planes be investigated.

The state of stress at a point is specified by six quantities, three normal stresses and three shearing stresses across the planes on which the normal stresses act. As the effect of an isotropic stress is only to change the initial index of refraction, it cannot be detected by a photoelastic pattern and therefore only the differences between the normal stresses plus the three shearing stresses, or the difference between the principal stresses and the planes on which they act, can be found. Without *a priori* knowledge as to the state of stress, five independent measurements must be made to determine the unknown quantities.

Let a plane be chosen. Consider some line in the plane as a reference direction. If a narrow beam of circularly polarized light is passed in the plane so that the wave normal is first in the direction of the reference line, then at one angle to it and next at another, and photographs are taken of the light scattered at right angles to the wave normals, three independent measurements will have been made for each point in the plane. Call the reference line the x axis, the plane the xy plane. The fringe spacings obtained for three positions of the wave normal do not completely determine the state of stress. Two more independent measurements are required to get $\sigma_x-\sigma_y$, $\sigma_y-\sigma_z$, τ_{xy}, τ_{yz}, τ_{zx}. Two positions of the wave normal in the xz plane other than along x will supply the additional information required. If, however, the orientations of the secondary principal stresses can be determined or are known, one need work only in the xy plane, the three fringe spacings and the orientations are sufficient.

The general problem of finding the orientation of the secondary or primary principal stresses is rather complicated. If the rotation ratio is small at all points, then plane polarized light entering along a direction of principal stress will indicate the directions of principal stress all along the wave normal. Only when the entering light is vibrating in such a direction will a continuous dark band appear. If the ratio is large, no such reliable way is available. A continuous dark band will not exist, even the entering direction of the principal stresses cannot be determined. Distinctness of fringe patterns cannot be used as a criterion; minimum distinctness does not necessarily occur when the observer is looking along a principal stress direction, and in general it would be difficult to determine such a minimum with any degree of exactness.

Fortunately, in the majority of cases the ratio of rotation to retardation will be small and the directions of the principal stresses can probably be determined.

Analysis of Plane Stress

In plane stress, the magnitude and direction of a principal stress is known at every point, ($\sigma_z=0$ acts perpendicular to the plane of the model). There are thus only three quantities to be determined, the principal stresses in the plane, σ_1, σ_2, and their orientation.

Consider rectangular axes x, y in the plate (Fig. 3). σ_y, the normal stress in the y direction, is determined from the fringe spacing when light is passed in the x direction, σ_ξ and σ_η when the wave normal is at two other known orientations with respect to the x axis. Taking these positions symmetrically about x, at some angle γ to it, and calling the distance between fringes obtained along these directions d_x, d_ξ, d_η, we have $\sigma_y=C/d_x$, $\sigma_\xi=C/d_\xi$, $\sigma_\eta=C/d_\eta$. The three normal stresses determine the principal stresses and their orientation in the plane. If γ is taken as 60°, the formulas become rather simple. They are entirely analogous to those developed for the equiangular strain rosette.[6]

$$
\begin{aligned}
\sigma_1&=\frac{C}{3}\left(\frac{1}{d_x}+\frac{1}{d_\xi}+\frac{1}{d_\eta}\right)+\frac{\sqrt{2}}{3}C\left[\left(\frac{1}{d_x}-\frac{1}{d_\xi}\right)^2+\left(\frac{1}{d_\xi}-\frac{1}{d_\eta}\right)^2+\left(\frac{1}{d_\eta}-\frac{1}{d_x}\right)^2\right]^{\frac{1}{2}},\\
\sigma_2&=\frac{C}{3}\left(\frac{1}{d_x}+\frac{1}{d_\xi}+\frac{1}{d_\eta}\right)-\frac{\sqrt{2}}{3}C\left[\left(\frac{1}{d_x}-\frac{1}{d_\xi}\right)^2+\left(\frac{1}{d_\xi}-\frac{1}{d_\eta}\right)^2+\left(\frac{1}{d_\eta}-\frac{1}{d_x}\right)^2\right]^{\frac{1}{2}},\\
\tan 2\theta&=\sqrt{3}\left(\frac{1}{d_\xi}-\frac{1}{d_\eta}\right)\Big/\left(\frac{2}{d_x}-\frac{1}{d_\xi}-\frac{1}{d_\eta}\right),\\
\sigma_1-\sigma_2&=\frac{2\sqrt{2}}{3}C\left[\left(\frac{1}{d_x}-\frac{1}{d_\xi}\right)^2+\left(\frac{1}{d_\xi}-\frac{1}{d_\eta}\right)^2+\left(\frac{1}{d_\eta}-\frac{1}{d_x}\right)^2\right]^{\frac{1}{2}},\\
\sigma_1+\sigma_2&=\frac{2}{3}C\left(\frac{1}{d_x}+\frac{1}{d_\xi}+\frac{1}{d_\eta}\right).
\end{aligned}
\tag{17}
$$

[6] R. D. Mindlin, "The equiangular strain-rosette," Civ. Eng. **8**, 546 (1938).

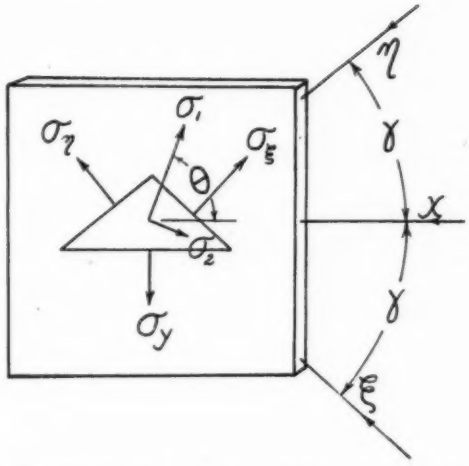

FIG. 3. Analysis of plane stress. Fringe spacings obtained from three positions of the wave normal in the plane determine the principal stresses and their orientation.

Similar formulas result for $\gamma=45°$.

As $\sigma_x+\sigma_y=\sigma_1+\sigma_2$, two measurements at right angles are sufficient to determine the sum of the principal stresses. It will be more accurate for two-dimensional work to take an isochromatic picture in the usual manner and then find the sum of the principal stresses as above, using the additional result as a check on the accuracy of measurement. For the principal stresses themselves, or for their sum and difference, care will have to be taken with the sign of the distance between fringes. If called positive when due to tension, it is negative when due to compression. The sign will often be apparent, if it is not, white light may be employed, the color sequence will show whether the stress is of the same or opposite sign as the stress at the previous point, and following back to a known point, as for example one on the boundary, the sign can be determined. Due to dispersion, it may be necessary to reduce the load for this determination. The isoclinics can also be used for determination of the sign. In the case of plane stress, the variation of stress through the thickness is small and a wide beam of light can be employed. The wider beam will give a much greater intensity of scattered light and may therefore be desirable.

It should be noted that a sheet of photoelastic material may appear free from initial birefringence when observed in a circular polariscope and yet have a fairly high equivalent stress perpendicular to the plane, which may make it unsuitable for this proposed method.

A two-dimensional state of stress also exists at an unloaded plane boundary. An isochromatic picture can be obtained to a certain extent but it would have little accuracy. The principal stresses and their orientation can be found by the method and formulas, (17), given for plane stress.

A plane of symmetry or a principal plane in a three-dimensional case is very similar to the plane stress case. The quantities found from the three measurements at 60° will be the differences between the principal stresses and their orientations, which is all that one can expect to obtain. Calling the normal stress on the plane σ_z, just substitute $\sigma_1-\sigma_z$ for σ_1 and $\sigma_2-\sigma_z$ for σ_2 in (17).

THE FREEZING METHOD

The preceding development has all been applied specifically to the determination of the state of stress from the patterns produced by the light scattered from a plane. It applies also with but few modifications to the "freezing" method. In this method[7,8] the model is heated, loaded, then cooled under load. Most of the birefringence present when the model is under load at the elevated temperature remains after cooling, and it is not disturbed by careful sawing. Thin slices are cut from the model and analyzed. When the slice is placed in a polariscope, an integrated effect through the thickness is obtained. If the stress in the neighborhood of a point is constant, the fringe order appearing there when the slice is in a circular polariscope is

$$n=\frac{(\sigma_p-\sigma_q)t}{C}, \qquad (18)$$

where, as before, σ_p and σ_q are the secondary principal stresses in the plane perpendicular to the wave normal (in general not the plane of the slice), t is the thickness of the slice in the direction of the wave normal, and C is the stress-optical coefficient. The difference between the secondary

[7] G. Oppel, "Polarisationsoptische Untersuchung raumlicher Spannungs- und Dehnungszustände," Forschung auf dem Gebiete des Ingenieurwesens **7**, 240 (1936).

[8] M. Hetényi, "The application of hardening resins in three-dimensional photoelastic studies," J. App. Phys. **10**, 295 (1939).

principal stresses is therefore determined directly from the fringe order, their orientation can be obtained in the same way one obtains the isoclinics for a model under plane stress. If the fringe orders and the orientations are obtained for three different directions of the wave normal, all information possible as to the state of stress is determined. The method is entirely analogous to that indicated in the section on "Analysis of General States of Stress" and applies with possibly even more accuracy because of the greater ease of determination of the directions of the secondary principal stresses. Little difficulty is caused by a small stress gradient provided the directions of σ_p and σ_q remain unchanged along the wave normal.

Rotation of the slice about only one axis (can be taken in the slice) is required, and only three positions need be investigated in this rotation. Immersion in a liquid of approximately the same refractive index will eliminate reflections.

If the p and q axes do rotate, it should be possible to find the amount of this rotation in a plane polariscope if the stress is sufficiently high, and generally one is interested only in the highly stressed portions. As shown in the preceding work, plane polarized light entering along a principal stress direction will rotate with the principal stress axes and emerge practically plane polarized. Independent rotation of the polarizer and analyzer will find the orientations and the amount of rotation. The correction factor to the fringe order to find the stress is, as before, $1/S$. The difference between the secondary principal stresses is given by

$$\sigma_p - \sigma_q = \frac{nC}{t} \cdot \frac{1}{S}. \tag{19}$$

The corrected values for the differences between the secondary principal stresses and the orientations found as above should be used referred to the central plane of the slice.

Hiltscher[9] proposed analyzing the slice cut out from the model in a microscope point by point using convergent polarized light as one does in crystallographic investigations. If rotation of the principal axes through the slice is at all appreciable, the proposal does not appear practicable.

Conclusion

The investigation of the effect of rotation of the principal axes in planes perpendicular to the wave normal led to two important results:

(1) Rotation increases the relative phase retardation by a factor $S=(1+(2\varphi/\Delta)^2)^{\frac{1}{2}}$ which at times may be quite large. If the ratio $2\varphi/\Delta$ is not constant, the ratio of the increment in 2φ to the increment in Δ between fringes can be used in regions of high stress.

(2) At high stress, the light vector rotates with the principal stress directions, plane polarized light entering along a direction of principal stress will remain practically plane polarized in the direction of this stress through the entire model.

The method of working in planes rather than point by point should be of value for general states of stress when a large portion of the model is to be analyzed. In the particular case of plane stress it yields a purely optical method of determining the sum of the principal stresses, or the principal stresses themselves, over the entire model.

[9] R. Hiltscher, "Polarisationsoptische Untersuchung des raumlichen Spannungszustandes im konvergenten Licht;" Forschung auf dem Gebiete des Ingenieurwesens **9**, 91 (1938).

Atomic Distribution in Aluminum-Silver Alloys During Aging

CHARLES S. BARRETT AND ALFRED H. GEISLER*
Carnegie Institute of Technology, Pittsburgh, Pennsylvania
(Received June 17, 1940)

Laue photographs of aluminum-rich aluminum-silver crystals during aging at 20° and 150°C show more or less clearly defined streaks along certain zonal ellipses, in addition to the streaks caused by thermal agitation. These have been analyzed by stereographic and reciprocal lattice projections and are found to result from two-dimensional gratings parallel to planes of the form {111}. The streaks with 20° aging are more diffuse than with 150° aging; no streaks were found with 200° aging. When the precipitate lattice is fully developed, it yields sharp spots along the streaks at positions predicted from earlier studies of the Widmanstätten structure; preceding this state there exist very thin plate-like nuclei on randomly spaced {111} planes, which govern the orientation and shape of the fully developed precipitate. These may consist of (*a*) clusters of silver atoms or (*b*) imperfect lattices caused by (111) layers of atoms shifting parallel to themselves as required for the transformation from the face-centered cubic to the hexagonal close-packed lattice but with the shifting occurring on random planes, thus destroying the lattice periodicity normal to these planes.

INTRODUCTION

A NUMBER of instances have recently been discovered in which diffraction occurs with one of the three Laue conditions relaxed, the diffraction pattern resembling that of a two-dimensional, crossed grating. The phenomena accompanying precipitation in aluminum-rich aluminum-copper alloys are of this type. Guinier[1] and Preston[2] have shown that soon after an alloy is quenched from a temperature within the solid solution range a set of streaks begins to appear superimposed on the normal diffraction pattern. The streaks arise from two-dimensional gratings on planes of the form {100}—presumably from small plate-like clusters of copper atoms which are probably the nuclei of the θ' lattice. The clusters appear to be a few angstroms in thickness and several hundred angstroms in diameter and are dispersed at random through the matrix; as they lack periodicity in one dimension they give rise to diffraction maxima characteristic of two-dimensional gratings. As aging continues, the clusters become fully developed θ' and ultimately the stable precipitate, θ. Some difficulties were encountered in the complete analysis of the photographs until it was realized that thermal agitation also causes streaks in Laue photographs (in the radial direction) which must be taken into account.[3,4]

Hendricks[5] has recently studied closely analogous streaks in x-ray photographs of various micas and has shown that they are produced by the lack of lattice periodicity normal to the cleavage plane of the mica crystals. Bradley, Bragg and Sykes[6] have observed similar diffraction effects from submicroscopic lamellar arrangements of phases in iron-copper-nickel alloys with certain rates of cooling. Crossed-grating effects are also common in electron diffraction photographs of very thin crystals and crystalline deposits.

The following work is an analysis of Laue photographs of aluminum-rich aluminum-silver alloys during aging. It is shown that crossed-grating diffraction effects arise in the early stages of the precipitation process, somewhat as in the aluminum-copper alloys, but with important crystallographic differences. The crossed gratings are parallel to {111} planes of the solid solution in the present case, and are thus directly related to the habits of the precipitate crystals when they

* Aluminum Company of America Graduate Fellow.

[1] A. Guinier, Comptes rendus **204**, 1115 (1937); **206**, 1641 (1938); Nature **142**, 569 (1938). J. Calvet, P. Jacquet and A. Guinier, J. Inst. Metals **6**, 177 (1939).

[2] G. D. Preston, Nature **142**, 570 (1938); Phil. Mag. **26**, 855 (1938); Proc. Roy. Soc. **A167**, 526 (1938); Proc. Phys. Soc. **52**, 77 (1940).

[3] G. D. Preston, Proc. Roy. Soc. **172**, 116 (1939).

[4] W. H. Zachariasen, Phys. Rev. **57**, 597 (1940); S. Siegel and W. H. Zachariasen, Phys. Rev. **57**, 795 (1940).

[5] S. B. Hendricks, Phys. Rev. **57**, 448 (1940).

[6] A. J. Bradley, W. L. Bragg and C. Sykes, *Researches into the Structure of Alloys*, advance copy (Iron & Steel Inst. May, 1940).

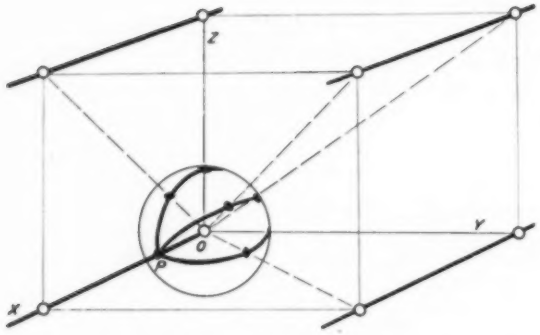

FIG. 1. Projection of reciprocal lattice points and lines onto reference sphere centered at the origin.

have grown to visible size, for Mehl and Barrett[7] have shown that they are then plate-like and parallel to {111} planes. On the other hand, aluminum-copper, which contains crossed gratings on {100} planes in the early stages of aging, shows plate-shaped precipitate crystals on {100} planes when they have grown to visible size.[8] Two different types of atomic arrangement that are capable of giving the effects are presented in the discussion.

EXPERIMENTAL PROCEDURE

Crystal preparation

An aluminum-silver alloy of 20.2 percent silver prepared by melting in a graphite crucible under a potassium chloride flux was cast into an iron mold, rolled to a reduction of 50 percent in thickness, and homogenized 48 hours at 550°C in lampblack. Large grains were grown by the strain-anneal method, cut out with a jeweler's saw, and thinned by careful rubbing on emery paper and by deep etching until the strained metal was removed. Crystals of chosen orientation were given a solution heat treatment of 18 hours at 560°C in lampblack, quenched in iced water, and aged for various times at temperatures between room temperature and 320°C.

X-ray photographs and their analysis

Laue photographs were found convenient for the work and were made with the general radiation from a cobalt target tube having Lindemann windows and operating at 37 kv. The low intensity streaks required exposures roughly ten times as long as the normal Laue spots.

For interpreting the Laue patterns, the reciprocal lattice is useful[9] and has been combined here with the stereographic projection which possesses some advantages over the usual gnomonic projection for the purpose.[10] Figure 1 is a sketch of the relations used. A reference sphere is centered at the origin of the reciprocal lattice, O, and the points of the reciprocal lattice are projected radially onto the sphere, as shown. These are projected, in turn, onto a stereographic projection by means of a projection point located on the surface of the sphere. The pole of a crystal plane on the reference sphere thus coincides with the radial projection of the reciprocal lattice point for that plane.

If there is a lack of periodicity of scattering power in the lattice so that one of the three Laue conditions is relaxed and diffraction effects are those of a two-dimensional grating, the reciprocal lattice contains lines normal to the plane of the grating. In Fig. 1 this condition is indicated for a grating in the YZ plane. Heavy lines parallel to X, normal to the YZ plane, are drawn through the reciprocal lattice points (since it is assumed that destruction of the third Laue condition leaves the others unaltered). The projection of these lines on the reference sphere is indicated in the figure, each point on the line being projected radially, as for the reciprocal lattice points. The

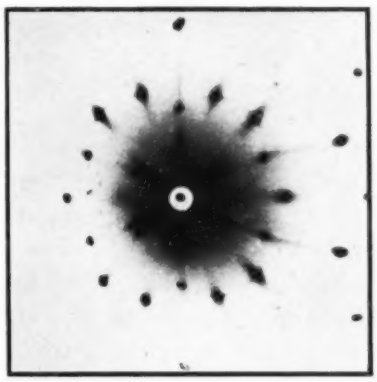

FIG. 2. Laue photograph of Al-Ag crystal aged 104 hours at 150°C, beam along [110], with [001] vertical.

[7] R. F. Mehl and C. S. Barrett, Trans. Am. Inst. Mining and Metallurgical Eng. **93**, 78 (1931).
[8] R. F. Mehl, C. S. Barrett and F. N. Rhines, Trans. Am. Inst. Mining and Metallurgical Eng. **99**, 203 (1932).
[9] C. C. Murdock, Zeits. f. Krist. **A99**, 205 (1938).
[10] C. S. Barrett, Trans. Am. Inst. Mining and Metallurgical Eng. **124**, 29 (1937).

projected lines on the reference sphere (and on its stereographic projection) are zone circles passing through the point P, the pole of the crossed grating.

Results

Figure 2 is a Laue photograph of an aluminum-silver crystal after quenching and aging 104 hours at 150°C. The x-ray beam was directed along the [110] direction. Each of the strong normal Laue spots is pierced by one or more streaks that lie along zonal ellipses. The geometry of these various streaks can be seen from the stereographic projection of the photograph, Fig. 3. (The method of plotting points along each streak is the same as if the points were strings of Laue spots.) It will be seen that all streaks follow great circles through the poles of planes of the type {111}, and correspond to the reciprocal lattice lines sketched in Fig. 4, which are parallel to directions of the form ⟨111⟩ in the reciprocal lattice; i.e., lines between (hkl) and $(h\pm1, k\pm1, l\pm1)$. Diffraction effects of this type would be produced by a set of crossed gratings arranged on the different {111} planes of the solid solution.

Figure 5 is a Laue photograph with the x-ray beam along a cubic axis. Its projection in Fig. 6 shows that the streaks follow zones through poles

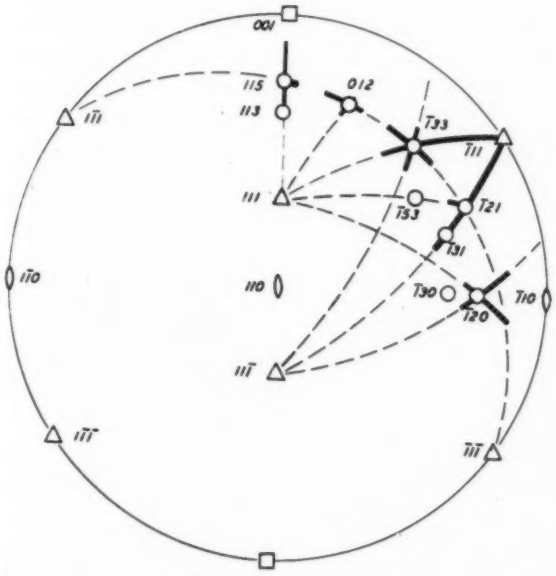

Fig. 3. Stereographic projection of one quadrant of Fig. 2 using scheme of Fig. 1. Crossed-grating streaks (heavy lines) follow zone circles (dashed lines) through {111} poles. Radial asterism from thermal agitation is neglected.

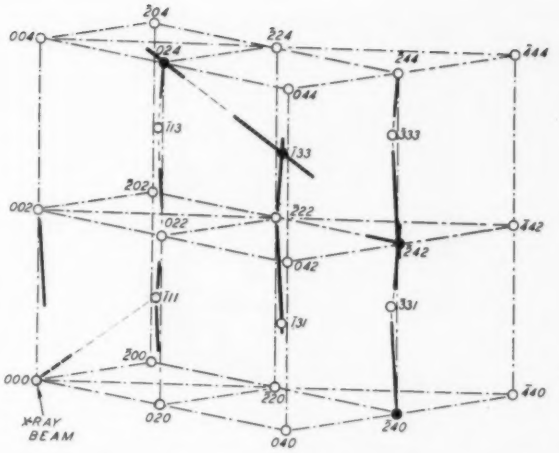

Fig. 4. Sketch of reciprocal lattice for Figs. 2 and 3. Lines between (hkl) and $(h\pm1, k\pm1, l\pm1)$ are drawn as heavy lines where they correspond to the observed streaks of the Laue pattern.

of {111} planes, as before. Photographs of other symmetrical and unsymmetrical orientations need not be reproduced here for they lead to the same conclusions.

The early stages of aging at low temperatures usually produce a somewhat different appearance in the Laue photographs; for example, Fig. 7 shows the appearance after fifty days at room temperature. A similar pattern was found in another crystal after one to four days aging at 150°C. Four intense but diffuse maxima occur at the three, six, nine, and twelve o'clock positions near the center. Other streaks form a double cross near the center, the axes of the cross lying 45° from the horizontal. These effects, however, can be accounted for on the same basis as the previous ones, if it is assumed that all streaks in the pattern are more diffuse than they are in Fig. 5. The greater width of the streaks through {131} spots causes them to overlap and blend with the thermal streaks at the three, six, nine, and twelve o'clock positions, and to diffuse into the background between these maxima and the {131} spots. The double cross can be ascribed to blending of several streaks which would correspond to great circles from (120) and $(\bar{1}20)$ poles to the four {111} poles.

On (110) Laue photographs the diffuse pattern contains radial rays extending out from the center and meeting the streaks through $(\bar{1}21)$ and $(\bar{1}33)$. In Fig. 4 these correspond to the dashed reciprocal lattice line from (000) toward $(\bar{1}11)$.

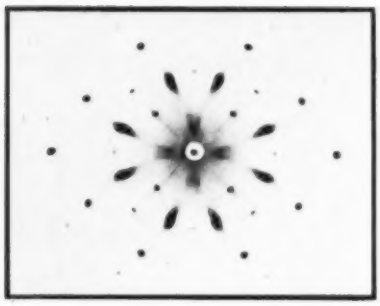

FIG. 5. Laue photograph of Al-Ag crystal aged 104 hours at 150°C, beam along [001], with [100] vertical.

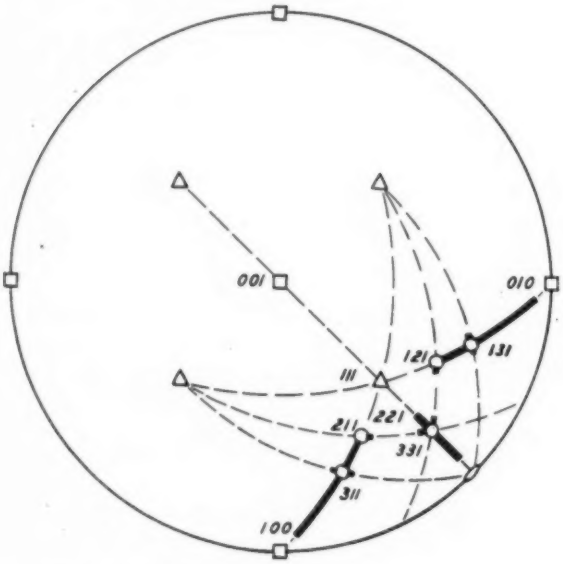

FIG. 6. Stereographic projection of one quadrant of Fig. 5.

Now this line is tangent at (000) to the reflection spheres for all wave-lengths and therefore could diffract only in the forward direction were it not for the diffuseness of the reciprocal lattice lines, which permits contact with the spheres out for some distance from the center. The intermediate state giving diffuse streaks was observed with aging at 150°C and below, but not at higher temperatures.

To show that Laue photographs are adequate to determine the plane of the two-dimensional grating, a Laue photograph of an aluminum-copper alloy is included, Fig. 8.* The alloy contained 4 percent copper and had been aged three days at room temperature after quenching; radiation from a silver target was directed along [110]. The prominent streaks differ from those in Fig. 2, and their analysis by stereographic and reciprocal projections, Fig. 9 and Fig. 10, confirm Preston's and Guinier's conclusion that the two-dimensional grating is on cube planes in this system. In Fig. 10 the reflection sphere for Ag $K\alpha$ is indicated; intersections of the sphere with the reciprocal lattice lines near (002), (024), ($\bar{2}42$) and ($\bar{2}20$) account for intensity maxima along the corresponding streaks in Fig. 8.

In the aluminum-silver experiments, when aging is continued for about three hours at 200° or for shorter times at higher temperatures, new spots begin to appear along the Laue streaks, as in Fig. 11. Powder photographs of the alloy at this stage show that the normal precipitate has formed. (The structure of the precipitate is hexagonal close-packed, with $a_0 = 2.879$, $c_0 = 4.573$, and has a random distribution of silver and aluminum atoms.[11]) This is confirmed by the stereographic projection of Fig. 11, one quadrant of which is reproduced in Fig. 12. The new spots fall as predicted by the orientation relationships derived by Mehl and Barrett,[7] namely, the (0001) plane of the precipitate parallel to {111} of the solid solution, with closest packed directions in these two conjugate planes parallel to each other.

If the distribution of intensity along the streak through (012) and ($\bar{1}$33) in Figs. 2 and 3 is noted, it will be seen that the intensity drops to a minimum at $\frac{1}{3}$ to $\frac{1}{5}$ of the distance from one Laue spot to the next. The wave-length along this streak is almost constant, so the blackening is

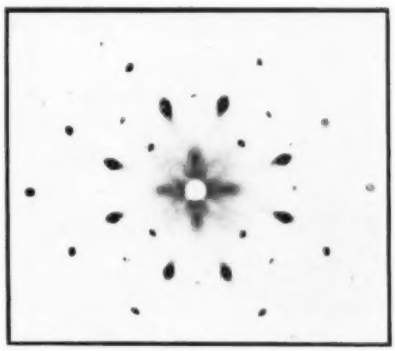

FIG. 7. Laue photograph of Al-Ag crystal aged 50 days at room temperature, beam along [001], with [100] vertical.

* This photograph was kindly given us by G. D. Preston, and is similar to, but more distinct than, some he has published.

[11] A. F. Westgren and A. J. Bradley, Phil. Mag. **6**, 280 (1928).

here more nearly representative of scattering power than in the case of the other streaks. By the principles of diffraction from a grating containing a small number of lines, it follows that the position of the minimum corresponds to a thickness of the diffracting layers in the neighborhood of three to five unit distances.

Powder photographs of polycrystalline samples quenched and aged for short times showed a few very weak extra lines not accounted for by either the solid solution or the precipitate. This indicates that a transition lattice[12] is playing a part in the mechanism, but the details are not yet clear.

Discussion and Conclusions

The evidence is conclusive for a type of crossed-grating diffraction from nuclei on the various {111} planes in the early stages of precipitation. The gratings appear to be between one and five unit cells thick with most heat treatments. Their lateral extent varies with the temperature of aging, and is of the order of 50 unit cells at room temperature and many times greater than this at 150°C, as is indicated by the width of the streaks.

Of what do the nuclei consist? Two possibilities are presented here, and still others may be possible. The first is the analog of the theory presented by Preston and by Guinier for aluminum-copper alloys, and the second is a derivative of the mechanism postulated by Mehl and Barrett[7] for precipitation in the aluminum-silver system, and similar to one that has been suggested by Thomson and Cochrane[13] to explain some anomalous effects in the electron diffraction from hexagonal close-packed metals that are transforming to their face-centered cubic modification.

The first theory is that silver atoms concentrate in thin plate-like clusters that lie parallel to various {111} planes in different regions of a solid solution crystal and that are spaced approximately at random. These clusters can be viewed as the first stage in the complex precipitation process,[14] identical with or followed by a stage in which a transition lattice, comparable to θ' in aluminum-copper alloys, is developed, and ultimately by the normal precipitate lattice. It has been argued[14] that these intermediate stages are the result of the complexities of atom movements by which the matrix lattice may transform to the equilibrium precipitate lattice under the crystallographic restraints imposed by the matrix lattice. As these alterations occur, the average size of the transforming regions is increasing—

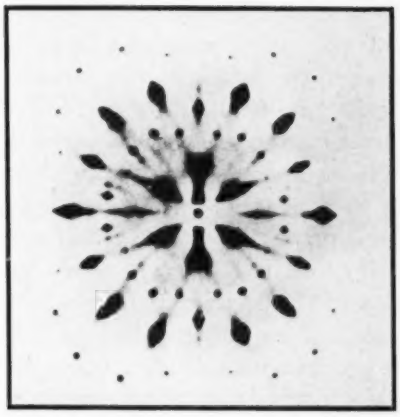

Fig. 8. Laue photograph of Al-Cu, 4 percent Cu, aged three days at room temperature, beam along [110], with [001] vertical.

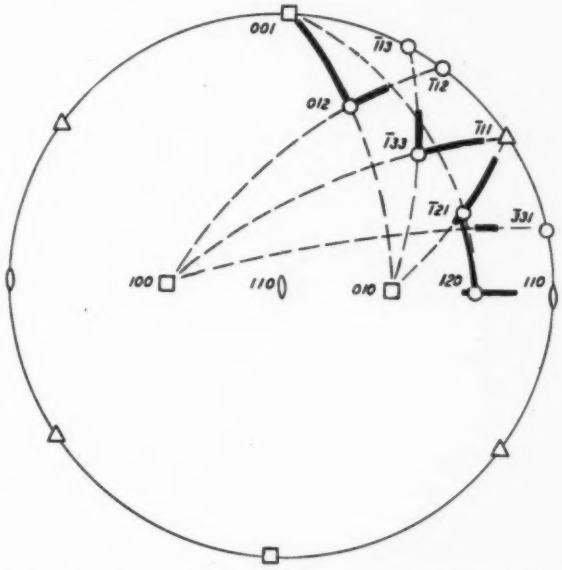

Fig. 9. Stereographic projection of one quadrant of Fig. 8. Crossed-grating streaks follow zone circles through {100} poles.

[12] L. Guillet and L. Guillet, Jr., Comptes rendus **209**, 79 (1939).

[13] G. P. Thomson and W. Cochrane, *Theory and Practice of Electron Diffraction* (Macmillan, 1939), p. 135.

[14] R. F. Mehl and L. K. Jetter, Preprint No. 30, October meeting (1939), American Society for Metals.

especially laterally. In any event, the basal plane (0001) of the precipitate can form from the (111) plane of the face-centered cubic matrix by merely shifting certain of the (111) layers of atoms parallel to themselves, and without altering the directions of the closest packed strings of atoms in these planes.[7] In different regions of a crystal, this process occurs on different planes of the {111} type, and in each region a distinct orientation of the precipitated crystallite occurs, giving a total of four orientations for the precipitate. The precipitated particles retain their plate-like habit in growing to a visible size, and produce a Widmanstätten pattern of thin plates on {111} planes. This, in connection with the analogous behavior in aluminum-copper alloys[8] (in spite of the occurrence of a transition phase in the latter system) suggests that this is a general rule and lends new interest to microstructures of the Widmanstätten type.

The second theory for the origin of the crossed-grating pattern is that the phase transformation starts at a great number of randomly distributed nuclei. In the early stages of the aging process, the alloy consists, on this view, of thin lamellae of the hexagonal close-packed phase distributed at random spacings through the face-centered lattice parallel to (111) planes of the latter. This could result from local regions in which a (111) net plane glides over the plane next to it as in crystallographic slip in such a way that the atoms in one plane are no longer directly above

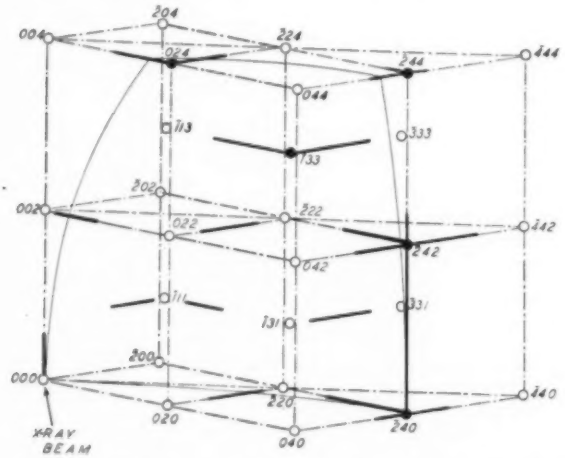

FIG. 10. Sketch of reciprocal lattice for Figs. 8 and 9. Lines between (hkl) and $(h\pm1,\ k,\ l)$, $(h,\ k\pm1,\ l)$ and $(h,\ k,\ l\pm1)$ are drawn as heavy lines where they correspond to the streaks of Fig. 8.

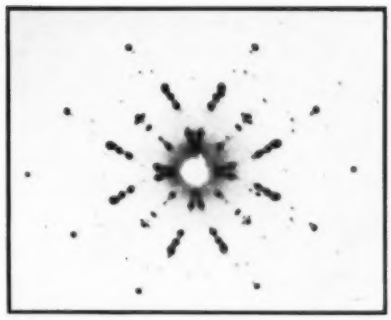

FIG. 11. Laue photograph of Al-Ag after precipitation (aged one hour at 320°C), beam along [100], and [001] vertical.

atoms in the third underlying plane.[7] The amount of the shift required for this is the distance between neighboring hollows in the close-packed array of atoms on the plane. If shifts of this kind take place with proper regularity, they alter the sequence of planes of the face-centered lattice, $ABCABC\cdots$, into the sequence for the hexagonal close-packed, $ABABAB\cdots$. If, on the other hand, shifting is random, it leads to a destruction of periodicity, for atoms will be directly over each other at distances nd where d is the spacing of (111) planes and $n=2,\ 3,\ 4,\ 5$ etc., at different places in the crystal. This will produce diffraction

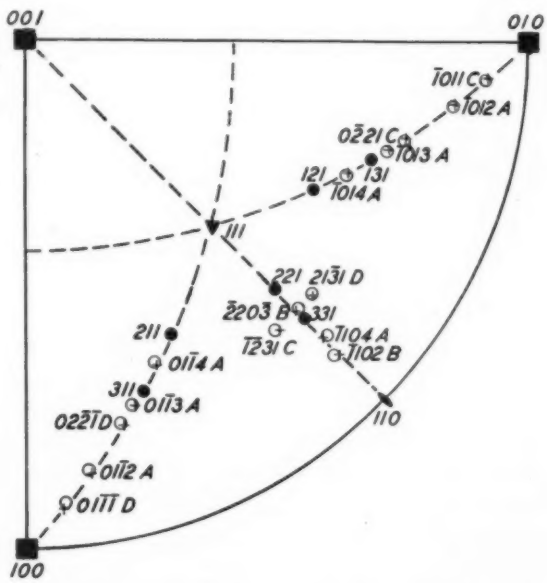

FIG. 12. Stereographic projection of Fig. 11. Crosses are calculated positions of poles of precipitate and open circles are observed positions; A refers to crystallites precipitated on (111) of matrix solid solution, B on $(\bar{1}\bar{1}1)$, C on $(1\bar{1}1)$ and D on $(\bar{1}11)$. Filled circles, triangles, and squares are poles of matrix solid solution.

effects such as we have observed, and analogous to those observed in the micas by Hendricks.[5] With further aging, a consistent scheme will replace the haphazard one in the same way that long-distance order replaces local order in superlattices, and sharp Laue spots from the precipitate lattice will appear along the streaks when some precipitate particles are large enough in all dimensions to give three-dimensional diffraction. When the precipitate has visible size, this process would be expected to produce the microstructures and Widmanstätten orientations actually observed.

Which of these two theories describes the pre-precipitation nuclei the more closely cannot be stated at present, nor can it be concluded that these are the only kinds of nuclei capable of explaining the diffraction effects. But, nevertheless, the essential features of the process are clear. In the early stages of aging there are plate-like nuclei of extreme thinness on randomly spaced {111} planes, and these govern the orientation and shape of the Widmanstätten precipitate. The nuclei consist of—or develop into—a transition phase which later decomposes into the stable precipitate.

Studies in Lubrication

IX. The Effect of the Pressure Variation of Viscosity on the Lubrication of Plane Sliders

M. Muskat and H. H. Evinger
Gulf Research & Development Company, Pittsburgh, Pennsylvania
(Received August 7, 1940)

The Reynolds theory is applied to the calculation of the lubrication properties of plane sliders—thrust bearings—of infinite width provided with lubricants whose viscosities increase exponentially with the pressure. The friction coefficient, minimum film thickness, and lubricant flow were calculated both for fixed wedge angle and pivoted sliders. The effect of the viscosity variation with pressure is determined by the magnitude of the dimensionless product of the viscosity-pressure exponent and the bearing load per unit area. The analysis shows that for each choice of this product there will be a limiting position of the pivot line of the slider or of the equivalent Sommerfeld variable at which the film pressures and friction forces will become infinite, and beyond which it will be impossible to operate the slider. Moreover this product is shown to be limited by a maximum value equal to 2, which means that the absolute maximum load per unit area which can be carried by such slider systems is equal to twice the reciprocal of the viscosity-pressure exponent. Specific calculations on the friction properties of bearings operating with lubricants of different viscosity pressure exponents give curves of friction coefficient *vs.* load or Sommerfeld variable quite similar to those observed in practical tests. At high loads or low values of the Sommerfeld variable the friction coefficient curves split and follow the behavior generally interpreted in terms of oiliness and boundary lubrication phenomena.

Introduction

In the last several years the question has been seriously raised as to whether or not the variation of the viscosity of a lubricant with the fluid pressure may play a significant role in bearing lubrication in which the loads are abnormally high. In particular, it has been proposed that in the operation of slow speed and heavily loaded journal bearings, such as are used in rolling mills, the high fluid pressures generated in the lubricant film may so increase the normal film viscosity as to change materially the lubrication behavior of the bearings. It has been known for some time that the viscosities of mineral oils are increased upon the application of high fluid pressures, but that the rise in viscosity due to this effect would be of importance in practical lubrication problems has only recently been considered seriously.

Among the first who have attempted to show specifically that the rise in viscosity with pressure can materially affect the performance of

lubrication systems are Bradford and Everett[1] and their collaborators. They showed that oils with different viscosity-pressure relationships would give different operating temperatures and load carrying capacities when used in lubrication systems under what were, otherwise, apparently identical conditions. Adding to their original interpretation, Givens[2] found that the temperature effects which they had observed with different oils could be directly related to the product of the viscosity-pressure coefficient and the load supported by the bearings.

Another comprehensive study of this problem has been made by Needs.[3] Needs measured directly the friction coefficient in a 120° centrally loaded fitted bearing as a function of the Sommerfeld variable[4] and load for a number of different lubricants, including mineral oil, castor oil, olive oil, and glycerine. In interpreting his experimental results, Needs assumed that his particular fitted journal bearing could be replaced by an infinitely wide slider or thrust bearing. He then found that, whereas the theory for such sliders operating with lubricants of fixed viscosity predicted friction coefficients decreasing monotonically with increasing load, his data showed that as the applied load per unit area was increased the friction coefficients dropped to minimal values and then began to rise with continued increase of the load. The values of the load at which the minima were observed varied with the character of the lubricant. Needs then worked out the hydrodynamic theoretical predictions for the variation of the friction coefficient with the Sommerfeld variable or bearing load of an infinitely wide slider for a lubricant whose viscosity increased exponentially with the pressure. The calculated friction curves for such systems were of exactly the same type as those he found experimentally. Although the quantitative agreement between the experiments and theory was not exceptionally striking, the general features of the two were in complete agreement, and the orders of magnitude of the loads at which the minima in friction appeared were correctly given by the calculations.

This concordance between the theoretical calculations and the experimental observations naturally appears to provide not only a confirmation of the physical foundations underlying the hydrodynamic theory of lubrication, but also suggests that the increase of viscosity with pressure may, under certain conditions, provide at least a partial explanation for the commonly observed rapid rise of friction coefficient with decreased Sommerfeld variable, which is usually interpreted as resulting from the breakdown of viscous lubrication and the development of boundary lubrication phenomena. However, upon closer analysis of Needs' theoretical considerations, it was found that the numerical calculations actually reported by Needs were restricted by severe limitations and assumptions. Specifically, all these calculations referred not only to a bearing 4″ in length in the direction of sliding, but, moreover, it was explicitly assumed that the bearing is always so tilted that the film thickness at the leading edge is twice that at the trailing edge. As will be seen later in this paper such an assumption is not only artificial but is, moreover, impossible to sustain in the operation of any practical bearing if the viscosity does vary with the pressure. Because of this situation it seemed necessary that the problem be generalized so as to make certain that even the qualitative agreement between theory and experiment so clearly exhibited in Needs' work was not entirely spurious. On the other hand, Needs' assumption that the sliders are of infinite width will be retained, since it has thus far not been possible to carry through all the necessary integrations for the finite width sliders.

Although, as will be seen below, it is, in principle, possible by a simple transformation to take into account the variation of the viscosity with pressure as given by any type of analytical function or even by numerical or graphical representations of the variation, we shall actually assume, as did Needs, an exponential variation of the viscosity with pressure. The basis for this assumption lies in the fact that the direct empirical measurements of the viscosity-pressure

[1] L. J. Bradford and R. S. Wetmiller, Mach. Design, **9**, 36–39 (January, 1937); H. A. Everett, Soc. Auto. Eng. J. **41**, 531, (1937); L. J. Bradford and C. G. Vandergrift, Inst. Mech. Eng. (General Discussion on Lubrication), 23–29 (1937).

[2] J. W. Givens, Ind. Eng. Chem. **31**, 1135 (1939).

[3] S. J. Needs, Trans. Am. Soc. Mech. Eng. **60**, 347 (1938).

[4] The "Sommerfeld variable" is used here to denote the product of the lubricant viscosity and journal speed divided by the bearing load per unit projected area.

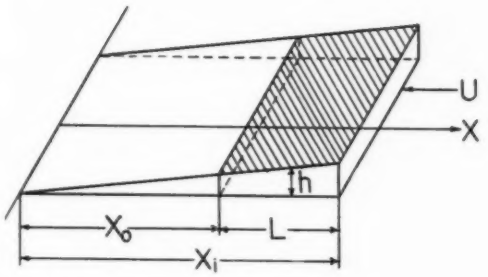

FIG. 1.

variation are generally best fitted by an exponential relation. Perhaps the closest correspondence between the empirical data and an exponential representation is that reported in the study of Hersey and Shore,[5] where the deviations of the semilogarithmic plots from linearity were generally rather small, and in some cases within the limits of the experimental errors. These data covered pressures to 4000 kg/cm² and temperatures to 140°C.

In the present investigation it has, therefore, been explicitly assumed that the relation between the viscosity and pressure is given by the equation:

$$\mu = \mu_0 e^{cp}, \tag{1}$$

where μ_0 is the viscosity at atmospheric pressure, and c is the vicosity-pressure exponent. The unit for the viscosity will be taken as the poise, and the pressure will be measured in kg/cm². In these units, the published data give a range for c of 5×10^{-4} to 3.5×10^{-3} cm²/kg. In general, c decreases with increasing temperature although the degree of variation with temperature is markedly different with different lubricants. The value of c is in general greater for the mineral oils than for the fatty oils.

Analytical Theory for Sliders of Infinite Width

Using the notation of the seventh paper of this series[6] on sliders of finite width with fixed viscosity, we may write down at once the Reynolds equation for the infinite slider as

$$\frac{d}{dx}\left(\frac{h^3}{\mu}\frac{dp}{dx}\right) = -6U\frac{dh}{dx}, \tag{2}$$

where (cf. Fig. 1) x is measured in the direction of motion, U is the velocity of the sliding plate, h is the film thickness, and μ is the lubricant viscosity, to be considered as a function of the film pressure p.

Now, in principle, as previously indicated, any preassigned mode of variation of the viscosity with the pressure can be formally taken into account in the solution of Eq. (2) or the general Reynolds equation by simply introducing the new variable defined by

$$\Psi = \int_0^p \frac{dp}{\mu(p)}, \tag{3}$$

which reduces Eq. (2) to

$$\frac{d}{dx}\left(h^3\frac{d\Psi}{dx}\right) = -6U\frac{dh}{dx}. \tag{4}$$

This is identical in form with Eq. (2), if, in the latter, we suppose the viscosity to be fixed. Hence, if we simply solve the lubrication problem under the assumption of fixed viscosity the pressure distribution for the system in which the viscosity is variable will be given immediately by the inversion of Eq. (3), that is, by expressing p as a function of Ψ according to Eq. (3).

Here, however, we shall carry through the analysis explicitly only for a viscosity-pressure variation defined by Eq. (1), since, as we have already seen, the latter affords a reasonable approximation to the empirical data on the viscosity pressure relationship. The explicit transformation between Ψ and p as defined by Eq. (3) will, therefore, be given for our case by

$$\Psi = (1/\mu_0 c)(1-e^{-cp}). \tag{5}$$

To solve Eq. (4) we now introduce the assumption that the film thickness h varies linearly with the distance x, that is,

$$h = mx. \tag{6}$$

To fix the boundary conditions we note that since at the coordinates x_i and x_0, defining the limits of the lubricant film, the pressure (above atmospheric) must reduce to zero, the function Ψ must also vanish at these boundaries, in view of the definition of Eqs. (3) and (5). We thus

[5] M. D. Hersey and H. Shore, Mech. Eng. **50**, 221 (1928). Cf. also R. B. Dow, J. App. Phys. **8**, 367 (1937), and M. D. Hersey, *Theory of Lubrication* (John Wiley, New York, 1938).

[6] M. Muskat, F. Morgan, and M. W. Meres, J. App. Phys. **11**, 208 (1940).

have at once for the function Ψ the solution

$$\Psi=\frac{6U}{m^2(x_i+x_0)}\frac{(x_i-x)(x-x_0)}{x^2}. \tag{7}$$

This solution, combined with Eq. (5), gives directly the explicit form for the pressure distribution in the film.

To obtain the various derived properties of the system it is necessary only to carry through the appropriate integrations. First, however, it is convenient to introduce the following notation:

$$\beta=\frac{6c\mu_0U}{m^2(x_0+x_i)};\quad \rho=\frac{x_i}{x_0};\quad S=\frac{\mu_0U}{W};\quad \bar{c}=\frac{cW}{L}, \tag{8}$$

where W is the total load per unit width supported by the lubricant film and L is the slider length in the direction of motion, namely, x_i-x_0. The dimensionless function S once more appears in the analysis here as characterizing the composite dynamical reaction of the lubricant film, and is analogous to the similar dimensionless quantity appearing in the study of the journal bearings, and which has been termed the "Sommerfeld variable." The dimensionless quantity $\bar{c}$ is a new variable introduced by the effect of the pressure variation of the viscosity, and its composition shows that for corresponding conditions of lubrication it is not merely the viscosity pressure exponent c which determines the behavior of the system but the product of c and the average film pressure W/L.

By making use of Eqs. (5) and (7), and carrying out the integrations, it is found that the load supported by the film may be expressed as

$$\frac{cW}{L}=\frac{c}{L}\int_{x_0}^{x_i}p\,dx=\bar{c}=\frac{4\rho}{R+(\rho+1)^2}\times\left[\frac{\rho+1}{\rho-1}\log\rho-\frac{2\sqrt{R}}{\rho-1}\tan^{-1}\frac{\rho-1}{\sqrt{R}}\right], \tag{9}$$

where β has been eliminated by introducing the auxiliary variable R defined by

$$R=4\rho/\beta-(\rho-1)^2. \tag{10}$$

The frictional forces may be obtained by integrating over the bounding surfaces the stress components

$$\sigma=\mu U/h\mp\frac{h}{2}\frac{\partial p}{\partial x}, \tag{11}$$

where the upper sign refers to the moving plate and the lower one to the stationary slider. If these integrations are carried out, and the frictional force be divided by the force normal to the plate, the coefficient of friction, f, for the moving slider is found to be given by

$$\frac{f}{m}=\frac{1}{2}+\frac{1}{R}\left[\frac{2\rho}{3\bar{c}}\left(\frac{\rho+1}{\rho-1}\right)\log\rho-\frac{(\rho+1)^2}{6}\right]. \tag{12}$$

In the case of the pivoted slider, it is necessary to know the position of the center of pressure. This is found by imposing the condition that the summation of moments about the center of pressure vanishes. If Δx denotes the distance of the center of pressure from x_0, it is given by

$$\frac{\Delta x}{L}=\frac{1}{WL}\int_{x_0}^{x_i}(x-x_0)p\,dx=\frac{1}{(\rho-1)^2}\cdot\frac{2\rho}{\bar{c}[R+(\rho+1)^2]}\times[(\rho^2-1)(1+\bar{c})-2\rho\log\rho]-\frac{1}{\rho-1}. \tag{13}$$

Another interesting property of the slider is the lubricant flow between the sliders. This is given by the basic hydrodynamic expression for the liquid flow between parallel plates, and from which Eq. (2) was derived. For the pressure distribution appropriate to the case under consideration this is equal to

$$Q=\frac{Uh}{2}+\frac{h^3}{12\mu}\frac{\partial p}{\partial x}=\frac{mU\rho L}{\rho^2-1}. \tag{14}$$

The minimum film thickness, h_0, is given simply by:

$$h_0=mx_0=mL/(\rho-1). \tag{15}$$

An auxiliary relation, useful in subsequent numerical calculations, may be obtained from Eqs. (8) and (10). By suitable substitutions

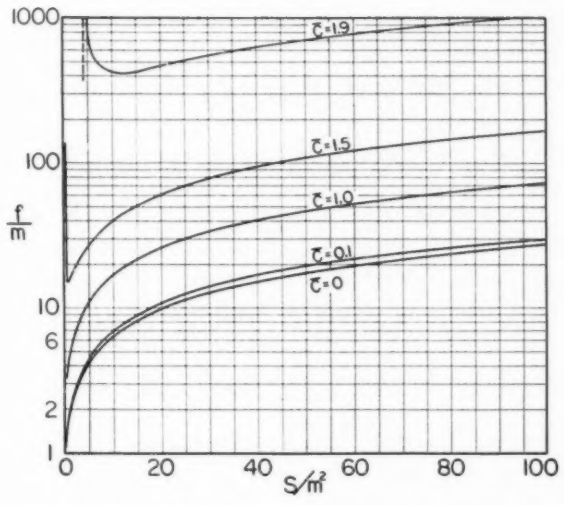

FIG. 2. The variation of f/m with S/m^2 for an infinitely wide slider operating with a lubricant whose viscosity increases exponentially with the pressure. f=friction coefficient; m=slope of slider; $S=\mu_0 U/W$; μ_0=lubricant viscosity at atmospheric pressure; U=slider speed; W=load per unit width; $\bar{c}=cW/L$; c=viscosity-pressure exponent; L=slider length, in the direction of motion. Dashed line is asymptotic limit of S/m^2.

making use of these relations it may be shown that

$$S/m^2=\frac{2\rho}{3\bar{c}}\left(\frac{\rho+1}{\rho-1}\right)\frac{1}{R+(\rho-1)^2}. \qquad (16)$$

It should be noted that the quantity R was introduced merely as a convenience in writing some of the formulae. However, it turns out that its use also facilitates the numerical calculations.

In order to obtain the numerical values shown graphically by the following curves, it was necessary to calculate sets of values of $\bar{c}$, R, and ρ, which satisfy Eq. (9) and then to substitute these values into the formulae for the derived properties of the slider. Since $\bar{c}$ was held constant for these curves, the most direct procedure was, of course, to substitute the desired value of $\bar{c}$ into Eq. (9) and then to find values of R and ρ satisfying the equation. Newton's method of approximation was employed for this purpose. For the curves presented in the next section in which the basic abscissa variable is S/m^2, the calculations essentially consisted of an elimination of ρ and R between Eqs. (9), (16), and one such as Eq. (12) or (14) for the various derived properties. For the section on the pivoted sliders the same type of elimination was carried out except that Eq. (13) rather than Eq. (16) was used to give the desired values of the abscissa variable.

PLANE SLIDERS WITH FIXED WEDGE ANGLES

As indicated by Eq. (16), the quantity S/m^2 enters the formulae determining the properties of a plane slider as a unit. However, it will be essentially equivalent to the directly observable quantity S itself if we consider the slider slope m to be fixed. From this point of view, the quantity f/m, as given by Eq. (12), may also be considered as representing directly the friction coefficient. In the next section, graphical representations of the properties of sliders will be given in which the sliders will be permitted to rotate about a pivot set along the center of pressure, and to assume various slopes depending upon conditions of operation.

By the methods outlined above, calculations were made of the friction coefficient, given by Eq. (12), *vs.* S/m^2. The results are plotted in Fig. 2 for various values of $\bar{c}$. The curve $\bar{c}=0$ corresponds to the slider operating with a lubricant of fixed viscosity. It will be seen that with increasing values of $\bar{c}$, that is, increasing viscosity pressure exponent, if the load be taken as fixed, the friction coefficient increases, although the general variation with S/m^2 for the larger values of the latter is very similar to that for the case $\bar{c}=0$. This rise in the friction coefficient with increasing $\bar{c}$ is clearly due to the rise in lubricant viscosity within the film resulting from the fluid pressures, which in turn require increased shearing forces in order to maintain the slider velocity U.

At the low values of S/m^2 the curves for $\bar{c}>0$ show a radically different behavior than the curve for $\bar{c}=0$. Thus, whereas the latter continues to decrease monotonically to the very limit, $S/m^2=0$, the curves for $\bar{c}>0$ fall to minimal values and then sharply rise again as S/m^2 continues to decrease. In fact, the friction coefficients rise to infinity and become asymptotic to lines parallel to the friction axis at definite limiting values for S/m^2. This peculiar behavior is the direct consequence of the general analysis of the previous section, and merely represents the fact that at these asymptotic limits the maximum

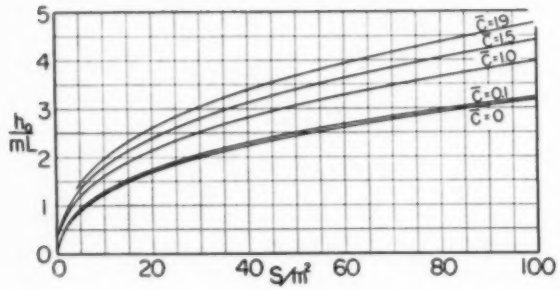

FIG. 3. The variation of the minimum film thickness h_0 with S/m^2 for an infinitely wide slider operating with a lubricant whose viscosity increases exponentially with the pressure. Notation as in Fig. 2.

film pressures and associated film viscosities become infinitely high so that no further increase in load or decrease in S is permissible. This situation comes about analytically in the following manner. By combining Eqs. (5), (7), and (8) the pressure distribution in the film may be put in the form

$$e^{-cp}=\frac{1}{y^2}[(1+\beta)y^2-\rho y(\rho+1)+\beta\rho], \quad (17)$$

where $y=x/x_0$. Hence, in order for the film pressure p to be real and have any physical significance, the bracket in Eq. (17) must be zero or positive. Recalling the definition of R from Eq. (10), it is readily verified that the bracket will always be positive for real values of y if $R>0$. Now at the limiting value of R, that is, when $R=0$, we have from Eqs. (9) and (16):

$$\bar{c}=\frac{4\rho\log\rho}{\rho^2-1}; \quad \frac{S}{m^2}=\frac{2\rho(\rho+1)}{3\bar{c}(\rho-1)^2}, \quad (18)$$

which, upon the elimination of ρ, give the relation between the minimal value of S/m^2 and $\bar{c}$. Such an elimination shows, as can be inferred from Fig. 2, that the asymptotic limit for S/m^2 monotonically increases with increasing $\bar{c}$, though it does not exceed 0.1 until $\bar{c}$ becomes greater than 0.9.

A very interesting corollary of the first of Eqs. (18) is that since ρ must always be real and positive—in fact greater than 1—$\bar{c}$ can never exceed the value 2. The fact that the equation for $\bar{c}$, as given by Eq. (18), refers to the limiting value for R, namely, $R=0$, gives the maximum possible value for $\bar{c}$ under all conditions; for, by reference to Eq. (9) it will be seen at once that when $R>0$, the magnitude of $\bar{c}$ will be even less, for any fixed value of ρ, than that given by Eq. (18). This limitation in the range of $\bar{c}$ should be kept in mind in the consideration of the various curves, both of Fig. 2 and those of the later diagrams.

The variation of the minimum film thickness with S/m^2 and for different values of $\bar{c}$ is shown in Fig. 3. Here the rise in the values of h_0/mL with increasing $\bar{c}$ is clearly due to the fact that the increasing lubricant viscosity within the film makes it possible for the sliders to carry any given load or to operate with any fixed value of S/m^2 with a greater film thickness. In other words, the pressure increase in viscosity leads to an increased load carrying capacity for the lubricant film.

Two curves for the variation of the center of pressure with S/m^2 are shown in Fig. 4. Curves for the other values of $\bar{c}$ shown in the previous figures have been omitted because of the difficulty of keeping them separated on the scale used in the plotting. As a whole it appears from Fig. 4 that the position of the center of pressure is relatively insensitive to the effect of the film pressure on the lubricant viscosity. To the extent that it has any effect it leads to a displacement of the center of pressure toward the trailing edge. The reason for this displacement is that the increase of the film pressure due to the viscosity variation is greatest in the region between the trailing edge and the center of the slider, thus leading to a resultant decrease in the moments of the pressure and with it in the distance of the center of pressure from the trailing edge.

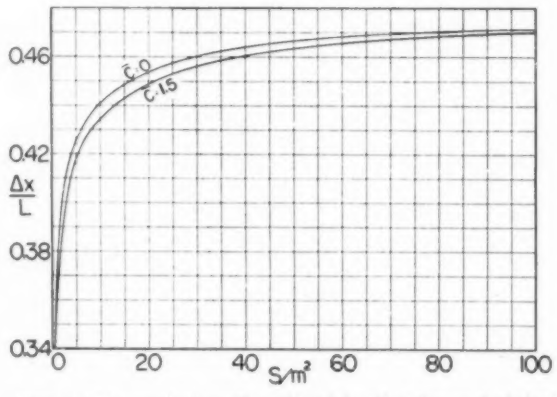

FIG. 4. The variation of $\Delta x/L$ with S/m^2 for an infinitely wide slider. Δx = distance of center of pressure from trailing edge. Rest of notation as in Fig. 2.

The variation of the lubricant flow with S/m^2 is plotted in Fig. 5. The rise in lubricant flow with increasing $\bar{c}$ is here caused by the increase in the film thickness already referred to. In fact, the effect of the larger film thickness is apparently more than enough to counterbalance the tendency for the lubricant flow to decrease because of the increased film viscosity.

Pivoted or Self-Aligning Sliders

In most practical thrust bearing installations the sliders are pivoted so as to permit the slope of the lubricant film to adjust itself to whatever the conditions of operation may happen to be. In order for such an adjustment of the slope to take place, it is clear that the center of pressure in the lubricant film must fall underneath the pivot line. In other words, the pressure distribution within the film and its associated properties must adjust themselves so as to give a center of pressure coinciding with the pivot line. The position of the latter therefore essentially determines the detailed behavior of the lubricant film for any preassigned set of operating conditions. For this reason, in discussing the problem of the pivoted slider it is convenient to use the position of the pivot line as the principal defining parameter of the slider system.

While it suffices to specify only the position of the pivot line to determine the lubrication properties of pivoted sliders operating with lubricants of fixed viscosity, it is necessary to assign also the value of $\bar{c}$ in case the lubricant viscosity varies with the pressure. The various derived

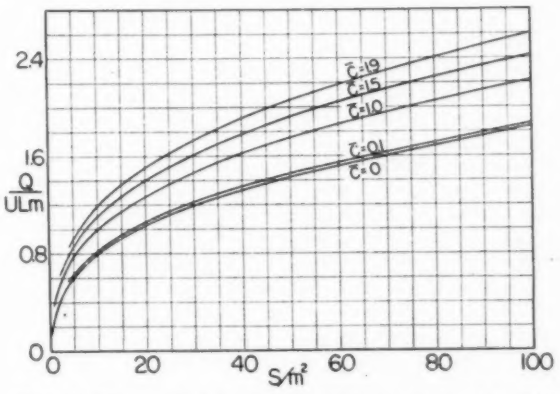

Fig. 5. The variation of the lubricant flow with S/m^2. Q=lubricant flow per unit width. Rest of notation as in Fig. 2.

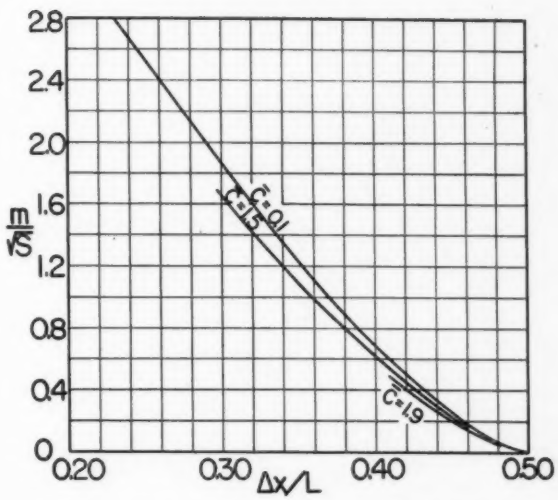

Fig. 6. The variation of the slope, m, of an infinitely wide pivoted slider operating with a lubricant whose viscosity increases exponentially with the pressure. $\Delta x/L$=(distance of pivot line from trailing edge)/(length of slider in the direction of motion). Rest of notation as in Fig. 2.

properties may, therefore, be plotted as a function of the position of the pivot line for fixed values of $\bar{c}$, or conversely.

The first derived property of interest for pivoted slider systems is that giving the slope assumed by the slider under various conditions of lubrication. It may be seen from Eqs. (16), (9), and (13) that this slope as well as the other derived properties of the lubrication system are essentially proportional to $\sqrt{S}$, if any equivalent pairs of the other auxiliary variables are kept fixed. It is, therefore, sufficient to calculate or plot directly the coefficients of proportionality, or the ratios between the derived quantity and $\sqrt{S}$.

The variation of $m/\sqrt{S}$ with the position of the pivot line is shown in Fig. 6. A small variation of $m/\sqrt{S}$ with $\bar{c}$ will be evident. The general decrease of $m/\sqrt{S}$ with increasing $\Delta x/L$ is quite similar to that obtaining with sliders of fixed viscosity. In fact, the curve for $\bar{c}=0$ has not been drawn on this figure because it would practically overlap that for $\bar{c}=0.1$. The limitation in the range of $\Delta x/L$ shown in Fig. 6 arises from the fact that the asymptotic limits of S/m^2 previously mentioned restrict the range of permissible $\Delta x/L$ to continually increasing limits as $\bar{c}$ is increased.

The variation of the friction coefficient for the pivoted sliders may also be expressed in terms of the ratio $f/\sqrt{S}$, which is given essentially by the

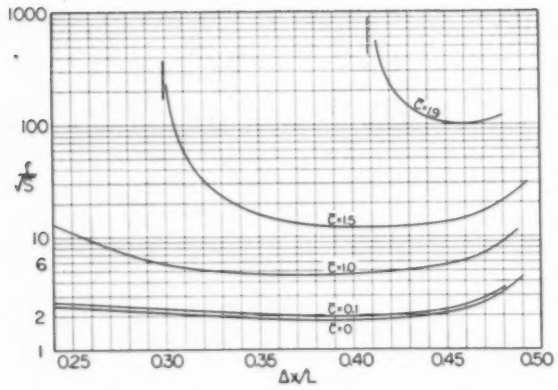

FIG. 7. The variation of the friction coefficient, f, of an infinitely wide slider with the pivot position. Dashed line is asymptotic limit for pivot position. Rest of notation as in Fig. 2.

product of the slope ratios of Fig. 6 and the ratio f/m of Fig. 2. The resulting curves plotted against $\Delta x/L$, with $\bar{c}$ kept fixed, is given in Fig. 7. This set of curves shows that increasing the quantity $\bar{c}$ will result in increasing values of the friction coefficient. As may be inferred from the earlier discussion of the sliders with fixed wedge angle, this behavior is a consequence either of the increased film viscosity with increasing viscosity pressure exponent, if the average load is considered as fixed, or the decreasing film thickness with increasing load if the viscosity pressure exponent be taken as fixed. As functions of $\Delta x/L$ the $f/\sqrt{S}$ curves all possess minima. However, with increasing $\bar{c}$ the position of the pivot line for minimum friction coefficient, and hence more efficient operation, is shifted closer to the center of the slider. In the limiting conditions where $\bar{c}=2$ the only permissible range of positions of the pivot line for stable operation apparently collapses and is shifted over to fall directly upon the center of the slider.

The variation of the minimum film thickness with the position of the pivot line for fixed values of $\bar{c}$ is shown in Fig. 8. With respect to the limitation of the ranges in $\Delta x/L$ appearing in these curves, the same remarks apply as previously made in connection with the function $m/\sqrt{S}$. The general increase of the minimum film thickness for fixed S and $\Delta x/L$ with increasing $\bar{c}$ again is an expression of the fact that the increased lubricant viscosity due to the film pressures permits the film to sustain the applied load with increasing film thickness, as would be expected from elementary considerations concerning slider systems operating with fixed viscosity lubricants. It will be noted from Fig. 8 that the $h_0/L\sqrt{S}$ curves show maxima when plotted against $\Delta x/L$. Moreover, to the extent that the permissible range of $\Delta x/L$ is large enough to allow for a full development of the maximum, the position of the latter shifts to decreasing values of $\Delta x/L$ as $\bar{c}$ is increased. Hence, in contrast to the situation with respect to the friction coefficient, the effect of the pressure increase of the viscosity would here indicate that the pivot line be shifted toward the trailing edge in order to maintain maximum values of the film thickness and hence reduce the tendency for metallic contact and rupture of the lubricant film.

The variation of the lubricant flow with $\Delta x/L$ for fixed values of $\bar{c}$ is shown in Fig. 9. Here, too, the curves as a whole show a trend which is in general parallel to that for the case $\bar{c}=0$, in which the lubricant viscosity is independent of the pressure. To the extent that the permissible range of $\Delta x/L$ permits a full development of maxima in the curves, the latter shift toward decreasing values of $\Delta x/L$ with increasing $\bar{c}$. The general increase of the lubricant flow with $\bar{c}$ must here, too, be interpreted as being essentially due to the increasing film thickness with which the system can operate as a result of the increase of viscosity with pressure.

In order to give a more practical representation of the significance of the various curves just presented, some calculations were carried through

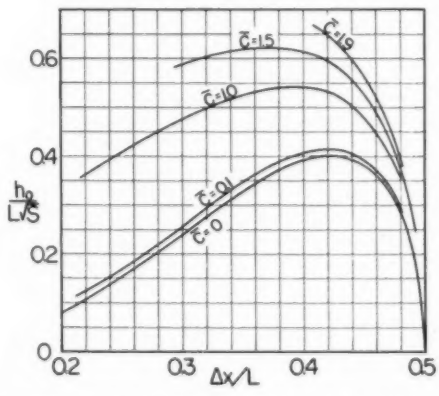

FIG. 8. The variation of the minimum film thickness, h_0, of an infinitely wide pivoted slider with the pivot position. Rest of notation as in Fig. 2.

on the properties of several slider systems operating under specific conditions. In all cases the atmospheric lubricant viscosity was taken as 1 poise, the slider velocity as 10 cm/sec., and the pivot positions, $\Delta x/L$, as 0.4. Calculations were then made for the variation of the friction coefficient and film thickness for three lubricants having viscosity pressure exponents of 0, 10^{-4}, and $2 \cdot 10^{-4}$ in.^{2}/lb. Since the atmospheric viscosity and slider speed were fixed, the only physical variation which would give a variation in S was that in the average load. In Fig. 10 the resulting friction coefficient as a function of the average load is plotted in terms of the composite variable S. In order to avoid having to specify the absolute value of the slider length in the direction of motion the products $f\sqrt{L}$ and $\sqrt{SL}$ were used as units. From Fig. 10 we see at once that, whereas for the lubricant whose viscosity is independent of the pressure the friction coefficient curve is a straight line passing through the origin, those for the lubricants with variable viscosity fall to a minimum and then rise steeply to infinity as S approaches its asymptotic permissible limit. This result is clearly very similar to, and suggestive of, the almost universal empirical observations with all types of lubrication systems, namely that as the characteristic variable corresponding to S continues to decrease the friction coefficients ultimately reach minimum values and then sharply rise to values which may be enormously greater than those at the minimum. It is generally considered and accepted that the passage through the minimum and subsequent sharp rise reflects a development of at least partial metallic contact and the incidence of boundary lubrication conditions. Here—as has also been pointed out by Needs—we find an exactly similar type of behavior under full viscous hydrodynamic conditions without having to invoke the complicating factors obtaining under boundary lubrication conditions. It will be seen, too, that the exact position of the minimum and the numerical values of the friction coefficient in the sharply rising portion beyond the minimum markedly depend upon the absolute values of the viscosity pressure exponent c, and in this way give a purely hydrodynamic analog of the so-called property of "oiliness." In particular, Fig. 10 shows that the lubricants with smaller viscosity pressure exponents will be more "oily" than those with high exponents, if one were to interpret the curves in terms of the oiliness phraseology. Of course, it is not proposed that in general the hydrodynamic effect of the increase in viscosity with pressure gives a real explanation of what are commonly termed boundary lubrication conditions or of the oiliness properties of the lubricants. However, in such systems where the loads may be exceptionally high, it may well be that the passage of the friction coefficient curve through a minimum and subsequent rise may be due, at least in part, to the purely hydrodynamic effect discussed here.

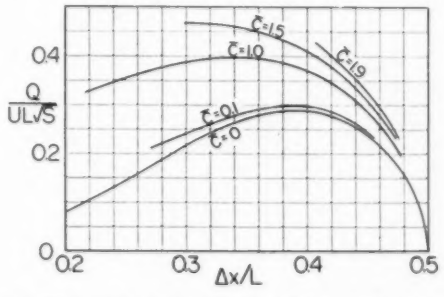

FIG. 9. The variation of the lubricant flow, Q, of an infinitely wide pivoted slider with the pivot position. Rest of notation as in Fig. 2.

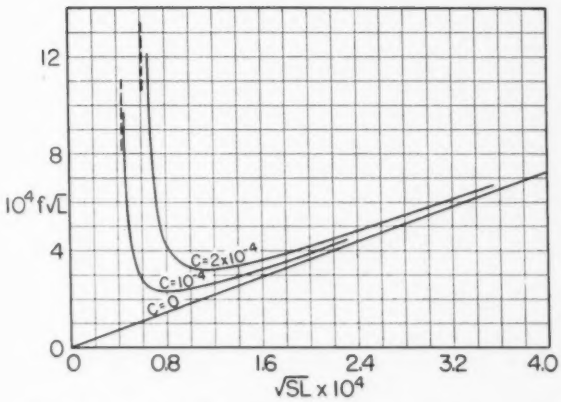

FIG. 10. The variation of the friction coefficient with S of pivoted sliders operating with three kinds of lubricant. Atmospheric viscosity = 1 poise for all lubricants; slider speed = 10 cm/sec. and pivot line distance = 0.4 of slider length in all cases; c = viscosity pressure exponent; dashed lines indicate asymptotes limiting permissible values of S. Rest of notation as in Fig. 2.

Corresponding to the higher friction coefficients indicated in Fig. 10 for the cases $c > 0$, the minimum film thicknesses will also be greater. In fact whereas the h_0 *vs.* $\sqrt{S}$ curve will pass linearly through the origin for $c = 0$, the film thickness for

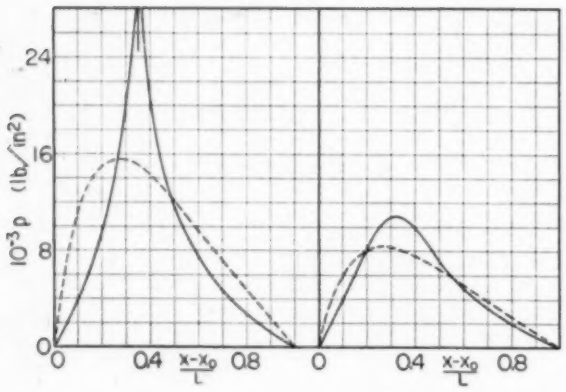

FIG. 11. The pressure distributions for the pivoted slider systems described by Fig. 10. For curves on left, average load = 9400 lb./in.²; for curves on right, average load = 5000 lb./in.²; for solid curves $c = 2\times10^{-4}$ in.²/lb.; for dotted curves $c = 0$ (const. viscosity); $(x-x_0)/L$ = (distance from trailing edge)/(slider length, in direction of motion).

$c > 0$ will always remain nonvanishing up to the asymptotic limits of S. Hence, while the sharp rise in the friction coefficient on passing the minimum would lead to high energy losses in the continued operation of the system, the fact that the film thickness remains relatively large and nonvanishing should give a compensating effect in avoiding the scoring and scuffing of the sliding surfaces.

The pressure distributions in systems corresponding to those represented by Fig. 10 are shown in Fig. 11 for $c = 0$ and $c = 2\cdot10^{-4}$ in.²/lb. For the curves on the left the average load is 9400 lb./sq. in., which is the maximum permissible for the lubricant of variable viscosity; the curves on the right correspond to an average load of 5000 lb./sq. in. It will be seen that the effect of the pressure increase of viscosity is to concentrate the normal film pressure rise to the region in the vicinity of the maximum obtaining in the film of constant viscosity. In fact, as indicated by the solid curve on the left, where the load is the maximum permissible, the film pressure theoretically rises to infinitely high values. At the low loads, of course, the whole effect is not so marked although it is still quite appreciable.

While Needs' theoretical work was pretty much limited to a presentation of curves of the type shown here in Figs. 10 and 11 for specific numerical cases, the corresponding results derived here are as a whole quite similar to those given by Needs. His explanation of his experimental observations, which show the same types of minima exhibited in Fig. 10, as being due to the effect of the pressure on the lubricant viscosity can therefore be accepted as sound. However, the present work does show that his specific assumption that the parameter ρ always has the value 2 is not justified. In particular, for the cases illustrated in Fig. 10 the value of ρ actually varies from a minimum of 1.0 to a maximum of 1.85. On the other hand, as indicated at the beginning of this paper, even the work presented here is based on the assumption that the sliders are of infinite width, whereas in practice they must, of course, always be of finite width.

It may be noted finally that the correlation observed by Givens between the temperature rise in the lubrication systems of Bradford and Everett and the product of the viscosity pressure coefficient and the load is quite consistent with the results of the present investigation. Although Needs did not point out the significance of this product, which has here been denoted by $\bar{c}$, the analysis of this paper shows that this quantity appears naturally as one of the defining parameters of the lubrication system. While this paper has not dealt with the temperature effects associated with the lubrication problem it is clear that these effects, too, will be ultimately determined by the composite quantity $\bar{c}$ rather than the load or viscosity pressure exponent separately. On the other hand, it should be noted that these same temperature effects within the lubricant film will tend to lower the effective values of the exponent c and thus extend the observed limiting load carrying capacities beyond those predicted on the assumption that c remains fixed. Moreover, the general lowering of the viscosity due to the internal film temperature elevations also will undoubtedly modify the pressure distributions and resultant integrated properties of the practical lubrication systems.

The authors wish to thank Dr. Frank Morgan for discussions of this paper, and Dr. Paul D. Foote, Executive Vice President, Gulf Research & Development Company, for permission to publish it.